Inorganic Chemistry

pubs.acs.org/IC Article

Telluracarbaporphyrins and a Related Palladium(II) Complex: Evidence for Hypervalent Interactions

Timothy D. Lash,* Deyaa I. AbuSalim, and Gregory M. Ferrence

Cite This: *Inorg. Chem.* 2021, 60, 9833−9847 Read Online

ACCESS | Metrics & More | Article Recommendations | Supporting Information

ABSTRACT: The reaction of a carbatripyrrin with a tellurophene dicarbinol in the presence of $BF_3{\cdot}Et_2O$, followed by oxidation with DDQ, afforded the first example of a telluracarbaporphyrin. Although this system exhibits strongly aromatic characteristics, it is prone to air oxidation, giving rise to a hydroxy derivative that was characterized by X-ray crystallography. The initial telluracarbaporphyrin reacted with palladium(II) acetate to give a stable organometallic complex, and X-ray crystallography showed that the palladium cation was coordinated to all four atoms in the CNTeN core. An oxacarbatripyrrin was also reacted with a tellurophene dialcohol to give an air-stable porphyrin analogue with a CNTeO core. Nonmetalated telluracarbaporphyrins showed relatively short Te−N separations that strongly implied the involvement of hypervalent tellurium interactions. Furthermore, despite the presence of a very large tellurium atom, the tellurophene subunit is not strongly pivoted away from the mean macrocyclic plane as would be expected in the absence of these interactions. The aromatic properties of heterocarbaporphyrins were assessed by proton NMR spectroscopy, NICS calculations, and AICD plots. In addition, the relative stability of hydroxytelluraporphyrins in comparison to their tellurophene oxide tautomers was investigated and the aromatic characteristics of these oxidized structures were evaluated.

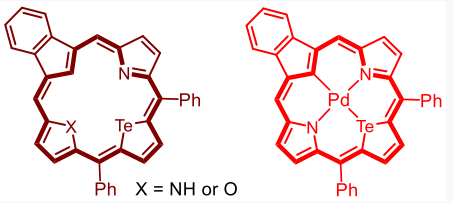

INTRODUCTION

Core-modified porphyrins have been widely investigated,[1,2] including oxa (**1a**)-, thia (**1b**)-, selena (**1c**)-, phospha (**1d**)-,[3] and carbaporphyrins (**2**) (Figure 1).[4] These systems exhibit unusual reactivity and modified spectroscopic properties, although many retain global aromatic characteristics that resemble those of true porphyrins. Telluraporphyrins (**1e**) are an interesting family of porphyrinoids that incorporate tellurophene subunits. The first example of this class, 21-tellura-23-thiaporphyrin **3**, was reported in 1978 but was isolated in very low yields.[5] Subsequently, efficient routes to telluraporphyrins such as **4** were reported (Figure 1).[6] Telluraporphyrin **4** is air-sensitive and can be oxidized with *m*-chloroperbenzoic acid to give the zwitterionic hydroxytelluraporphyrin **5** together with an oxaporphyrin (the latter product is derived from **5**).[6] Many examples of telluraporphyrins and heterotelluraporphyrins were subsequently reported,[7] including ditelluraporphyrins **6** (Figure 1).[8] Ditelluraporphyrins have unique properties, and the presence of two tellurophenes within the porphyrinoid framework results in one of the rings becoming inverted, although the inverted ring is strongly pivoted away from the macrocyclic plane. Treatment of **4** with hydrochloric acid afforded vacataporphyrin **7**,[9] and ditelluraporphyrins were used to prepare dideazaaporphyrins (divacataporphyrins).[10,11] Ditelluraporphyrins have also been used to generate metallaporphyrins such as **8a**,**b**.[12] Recently, investigations into telluraporphyrin-type structures have attracted renewed interest[13] and new examples have been reported, including tellurabenziporphyrins[14] and ditelluradiazuliporphyrins.[15]

Carbaporphyrinoid systems have been prepared by numerous synthetic strategies.[4,16] A recent innovation in the synthesis of carbaporphyrins involves the utilization of carbatripyrrin intermediates **9** that were easily prepared in three steps from indene (Scheme 1).[17] Indene reacted with KOH and pyrrole-2-carbaldehyde in refluxing ethanol to give fulvene **10**, and subsequent reduction with lithium aluminum hydride afforded the dihydro derivative **11**.[17] Further condensation with pyrrole-2-carbaldehyde gave carbatripyrrin **9a** (Scheme 1).

Under dilute conditions, mixtures of products were obtained, including isomeric derivatives **12a**, but under more concentrated conditions the relatively insoluble carbatripyrrin precipitates from solution and this drives the equilibrium toward the formation of tautomer **9a**.[17] Furfural similarly reacted with **11** under these conditions to give oxacarbatripyrrin **9b**.[18] Reaction of **9a** or **9b** with furan, thiophene, or selenophene dicarbinols **13a−c** in the presence of boron trifluoride etherate afforded the series of heterocarbaporphyrins **14a−c** and **15a−c** (Scheme 2),[17,18] including the first examples (**15b**,**c**) of porphyrin analogues with four different types of atoms within the macrocyclic core (CNSO and CNSeO, respectively).[18,19] Diphenyloxacarbaporphyrin **14a**

Received: April 11, 2021
Published: June 17, 2021

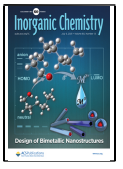

https://doi.org/10.1021/acs.inorgchem.1c01039
Inorg. Chem. 2021, 60, 9833−9847

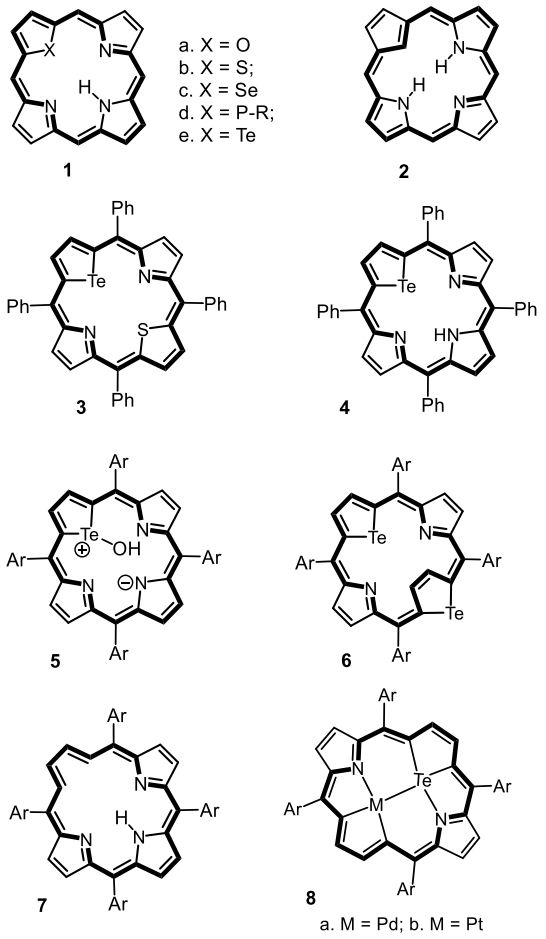

Figure 1. Telluraporphyrins and selected porphyrin analogues.

Scheme 1. Synthesis of Carbatripyrrins

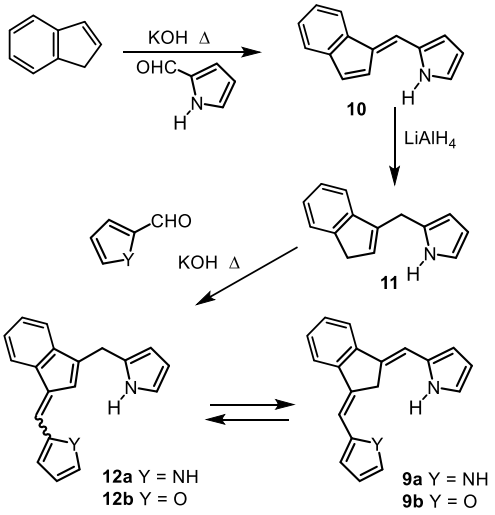

and diphenylthiacarbaporphyrin **14b** reacted with nickel(II) acetate or palladium(II) acetate to give organometallic derivatives **16a,b** and **17a,b** (Scheme 3).[2,21] When **14a** and **14b** were reacted with nickel(II) acetate in the presence of air, oxidation products **18a,b** were isolated.[20] Selenacarbaporphyrin **14c** failed to give isolable products with nickel(II) acetate but reacted with palladium(II) acetate to afford the palladium(II) complex **17c**.[20] The versatility of this chemistry suggests

Scheme 2. Synthesis of Heterocarbaporphyrins

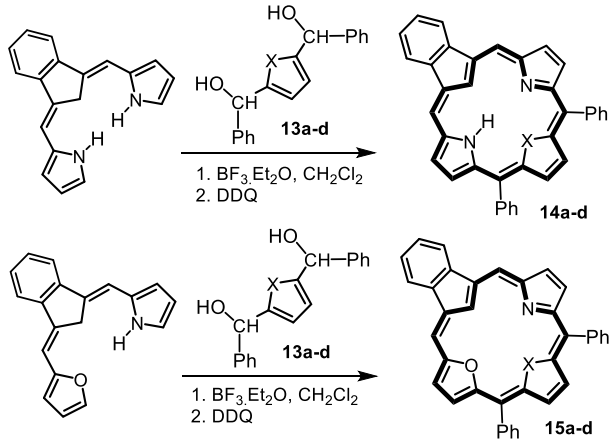

Scheme 3. Metalation and Oxidation of Heterocarbaporphyrins

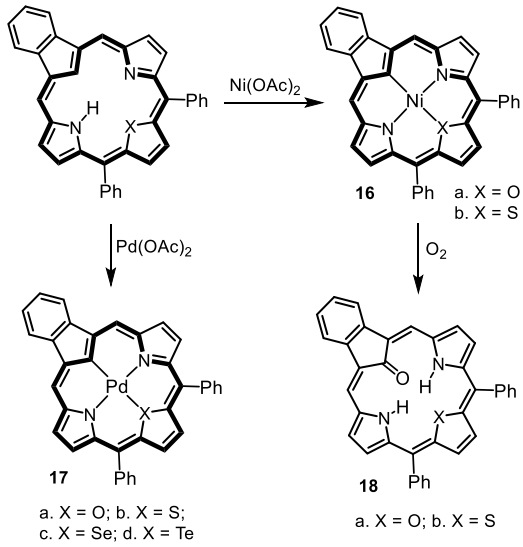

that further examples of heterocarbaporphyrins should be accessible using this approach.[18,19] In this paper, the first examples of telluracarbaporphyrins and a palladium(II) derivative are reported.

RESULTS AND DISCUSSION

Carbatripyrrin **9** was reacted with tellurophene dicarbinol **13d** under nitrogen in the presence of boron trifluoride etherate (Scheme 2). Following oxidation with 2,3-dichloro-5,6-dicyano-1,4-benzoquinone (DDQ), the targeted telluracarbaporphyrin **14d** was generated. Purification was achieved by column chromatography on basic alumina. However, solutions of **14d** proved to be unstable and readily oxidized in the presence of air.[22] It was anticipated that the presence of a large tellurium atom within a porphyrin-like framework would significantly distort the macrocycle and reduce the aromatic characteristics of the system. The UV−vis spectrum of **14d** gave a moderately strong Soret band at 446 nm with a broad shoulder at 556 nm and a series of poorly defined Q bands at higher wavelengths. In comparison to thia- and selenacarbaporphyrins **14b,c**,[17] the absorption bands are bathochromically shifted and relatively distorted (Figure 2) and this result is

https://doi.org/10.1021/acs.inorgchem.1c01039
Inorg. Chem. 2021, 60, 9833−9847

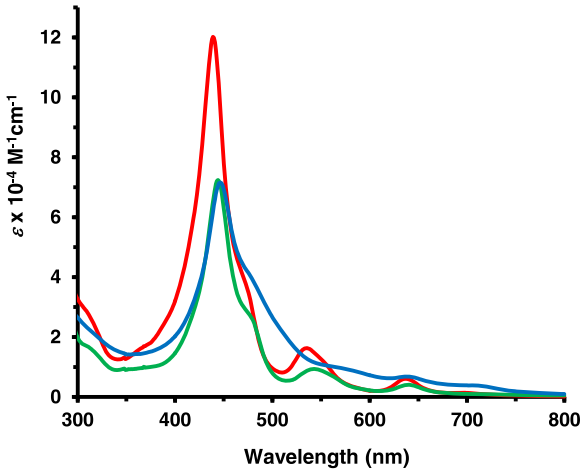

Figure 2. UV−vis spectra of thiacarbaporphyrin **14b** (red line), selenacarbaporphyrin **14c** (green line), and telluracarbaporphyrin **14d** (blue line) in 1% Et_3N−99% $CHCl_3$.

consistent with deformation of the π system. The addition of trace amounts of TFA gave rise to a new species, attributed to the monocation **14d**H^+ (Scheme 4), and this showed three

Scheme 4. Protonation of Telluracarbaporphyrins

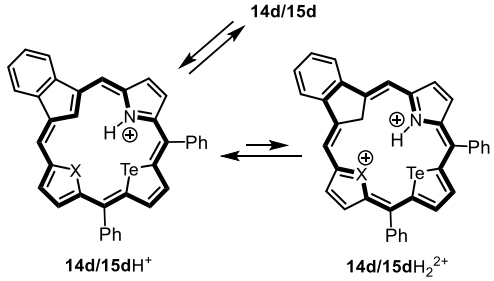

Soret-like bands between 400 and 600 nm and a broad absorption centered at 814 nm (Figure 3). In 10% TFA−90% chloroform, a strong Soret band emerged at 471 nm and this

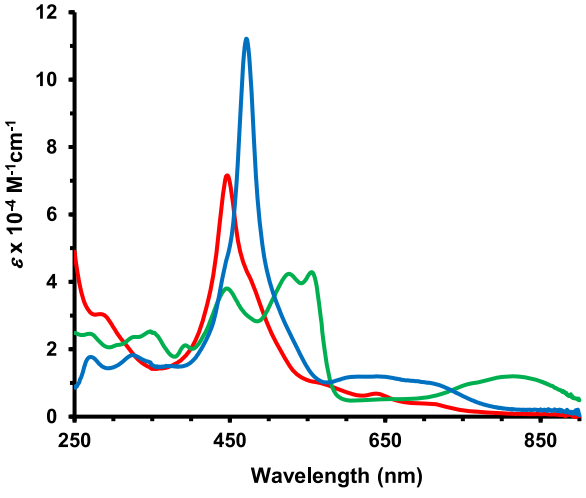

Figure 3. UV−vis spectra of telluracarbaporphyrin in chloroform (free base, red line), 0.1% TFA−99.9% $CHCl_3$ (green line, monocation **14d**H^+), and 10% TFA−90% $CHCl_3$ (dication **14d**H_2^{2+}, blue line).

was attributed to the formation of the dication **14d**H_2^{2+} (Scheme 4). The proton NMR spectrum for **14d** in $CDCl_3$ gave a 2H singlet for the *meso* protons (5,20-H) at 10.14 ppm, while the external pyrrolic protons afforded two 2H doublets at 8.94 and 8.60 ppm and the tellurophene protons produced a 2H singlet at 9.98 ppm. In addition, the internal C−H protons gave a 1H singlet at −2.58 ppm and N−H afforded a broad resonance at −2.21 ppm. These results demonstrate that telluracarbaporphyrin **14d** has a strong diamagnetic ring current that is consistent with an aromatic macrocycle. A comparison of the proton NMR data with oxa-, thia- and selenacarbaporphyrins **14a−c**[17] indicates that the diatropic ring current for **14d** is slightly reduced (Table 1), but the

Table 1. Selected Proton NMR Resonances (ppm) for Heterocarbaporphyrins 14a−d and 15a−d

	5,20-H	12,13-H	7,18-H	8,17-H	21-H
14a[17]	10.20	9.04	9.14	8.60	−4.31
14b[17]	10.23	9.55	9.07	8.73	−4.99
14c[17]	10.30	9.81	9.06	8.72	−4.49
14d	10.14	9.98	8.94	8.60	−2.58
19	9.97	10.33	8.94	8.49	−2.06
15a[18]	10.00, 10.16	8.81, 9.02	8.92, 9.41	8.47, 8.85	−3.75
15b[18]	10.13, 10.25	9.36, 9.59	8.99, 9.49	8.65, 9.11	−4.00
15c[18]	10.15, 10.24	9.65. 9.87	9.01, 9.44	8.68, 9.09	−3.86
15d	10.21, 10.26	10.13, 10.25	9.07, 9.50	8.68, 9.12	−2.58

relatively small changes to the upfield and downfield resonances imply that **14d** still retains a high degree of aromatic character. The carbon-13 NMR spectrum exhibited a significant amount of broadening that showed no improvement at 50 °C. The bridging methine carbons (5,20-CH) gave a resonance at 111.6 ppm, while the internal CH appeared at 117.9 ppm. The identity of **14d** was further confirmed by TOF ESI HR-MS.

Dilute solutions of **14d** in chlorinated solvents rapidly oxidized to give the related hydroxytelluracarbaporphyrin **19** (Scheme 5). This is illustrated for the UV spectra shown in Figure 4. After 1 h, conversion of **15** to **19** was virtually complete. Air oxidation was far less efficient for more concentrated solutions, but a clean conversion was obtained when solutions of **14d** were shaken with 0.1% aqueous ferric chloride for 5−7 min. The best overall results were obtained when the crude product from the reaction of carbatripyrrin **9**

Scheme 5. Air Oxidation of Telluracarbaporphyrin 14d

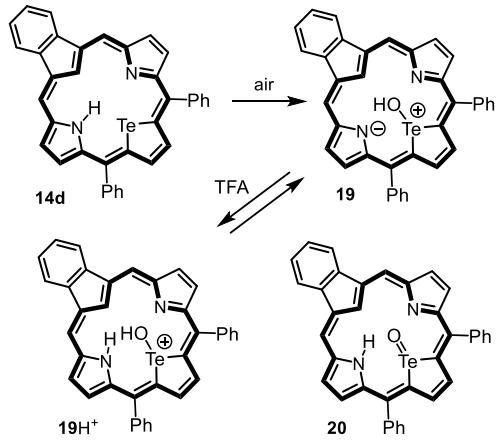

https://doi.org/10.1021/acs.inorgchem.1c01039
Inorg. Chem. 2021, 60, 9833−9847

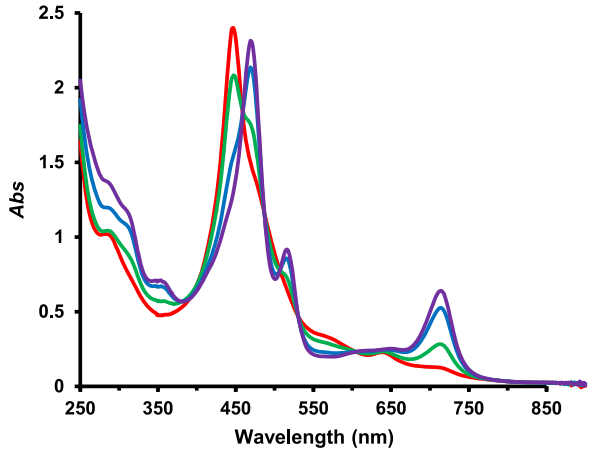

Figure 4. UV−vis spectra of **14d** (0.335 μM) in 0.05% Et_3N−99.95% chloroform after 0 min (red), 20 min (green), 40 min (blue), and 60 min (purple) showing the conversion of telluracarbaporphyrin **14d** into hydroxytellurophene derivative **19**.

with **13d** was shaken with the ferric chloride solution. The UV−vis spectrum for **19** in chloroform gave a strong Soret band at 470 nm and weaker absorptions at 313, 516, and 715 nm (Figure 5). Addition of trace amounts of TFA (10 equiv)

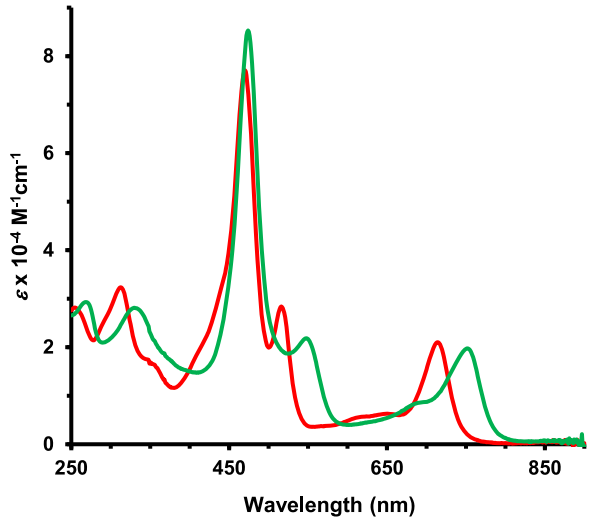

Figure 5. UV−vis spectrum of hydroxytelluracarbaporphyrin **19** in chloroform free base, (red line) and 0.05% TFA−99.95% chloroform (monocation $\mathbf{19}H^+$, green line).

gave a new species with a Soret band at 474 nm and additional absorptions at 330, 548, and 752 nm. This was attributed to the formation of monocation $\mathbf{19}H^+$. The proton NMR spectrum for **19** in $CDCl_3$ (Figure 6) showed the *meso* protons (5,20-H) at 9.97 ppm, while the tellurophene protons (12,13-H) were shifted downfield to 10.33 ppm (Table 1). The internal C−H gave a singlet at −2.06 ppm, while the O−H resonance appeared further upfield at −3.82 ppm. Significant shifts in these resonances were noted at higher concentrations, but the results clearly demonstrate that the system retains strongly diatropic characteristics. In the carbon-13 NMR spectrum, the 5,20-carbons appeared at 118.8 ppm and the internal C−H was identified as a resonance at 127.2 ppm.

In principle, the oxidation product could also be assigned to tellurophene oxide **20**. The structure of **19** was confirmed by X-ray crystallography, as this clearly identified the OH unit (Figure 7). Surprisingly, the molecular structure of **19** shows that the porphyrinoid is only slightly distorted from planarity. Relative to the mean 18-annulene plane, which includes both nitrogen atoms, the pyrrole rings are tilted 5.38(7) and 8.22(5)°, the indenyl moiety is canted by 5.12(3)°, and the tellurophene unit is rotated by −6.79(4)°. However, the rms distance all framework atoms lie from the mean 18-annulene plane is 0.125 Å with C21 0.213(3) Å above and Te atom 0.3253(3) Å below the mean plane. The distances between the tellurium atom and the two adjacent pyrrolic nitrogens are 2.521(2) and 2.587(2) Å, values that are consistent with the presence of covalent bonds to a hypervalent five-coordinate tellurium. This interaction may be responsible for the unexpected planarity of the ring system. With the exception of the Te−N, C1−C2, and C3−C4 bond lengths, a Mogul geometry check validated all bond distances to be within typical ranges.[23] The 1.482(4) Å (C1−C2) and 1.484(4) Å (C3−C4) bond lengths are longer than the average (1.45(1) Å) for fully delocalized indenyl systems and are consistent more with single-bond lengths, suggesting that the π system for the benzo unit is isolated from the main macrocyclic π system. The remainder of the framework has bond distances that are consistent with an overall aromatic 18-π-electron delocalization pathway.

The reaction of telluracarbaporphyrin **14d** with palladium(II) acetate in chloroform−acetonitrile at room temperature gave the dark red palladium(II) complex **17d** in 42% yield (Scheme 3). The best overall yields could be obtained by treating the crude product from the reaction of **9** and **13d** with palladium(II) acetate, and **17d** was isolated in 16% yield over the two reaction steps. Although palladium complexes of oxa-, thia-, and selenacarbaporphyrins have been reported previously,[20] the formation of a metal complex with a CNTeN coordination core is unique. The complex proved to be very stable but gave broad bathochromically shifted absorptions in its UV−vis spectrum in comparison to the related thia- and selenacarbaporphyrin complexes **17b,c** (Figure 8). The proton NMR spectrum of **17d** in $CDCl_3$ (Figure 9) shows that the macrocycle still possesses a diamagnetic ring current, as the *meso* protons (5,20-H) give rise to a downfield singlet at 9.76 ppm. However, the tellurophene protons (12,13-H) shifted upfield to 8.82 ppm, and the pyrrolic protons appeared as two 2H doublets at 8.76 and 8.25 ppm, indicating a decrease in the diatropicity of the macrocycle. At 32 °C, the phenyl groups gave very broad resonances between 6.5 and 7.5 ppm, but these coalesced at 55 °C (Figure 9). This observation indicates that the aryl substituents have hindered rotation. In the carbon-13 NMR spectrum, the bridging methine carbons (5,20-CH) gave a peak at 122.1 ppm, while the external tellurophene carbons (12,13-CH) produced a downfield resonance at 153.0 ppm.

The structure of palladium complex **17d** was confirmed by X-ray crystallography (Figure 10). In this structure, the tellurophene ring is strongly pivoted away from the mean macrocyclic plane. The palladium(II) center in **17d** resides in a distorted-square-planar coordination environment with 1.990(5) Å (Pd−C21), 2.077(5) Å (Pd−N22), 2.5468(5) Å (Pd−Te), and 2.062(5) Å (Pd−N24) bond lengths. The Pd−C and Pd−N bond lengths are similar to those observed for the analogous selenium-containing complex.[20] The 129

https://doi.org/10.1021/acs.inorgchem.1c01039
Inorg. Chem. 2021, 60, 9833−9847

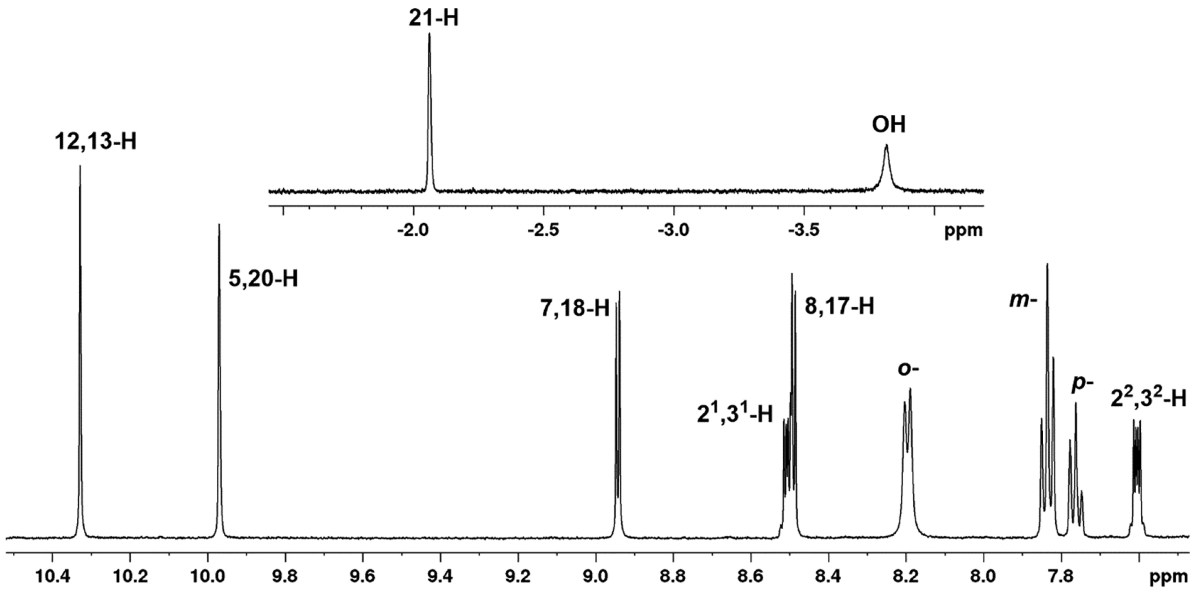

Figure 6. 500 MHz proton NMR spectrum of **19** in $CDCl_3$ at 50 °C.

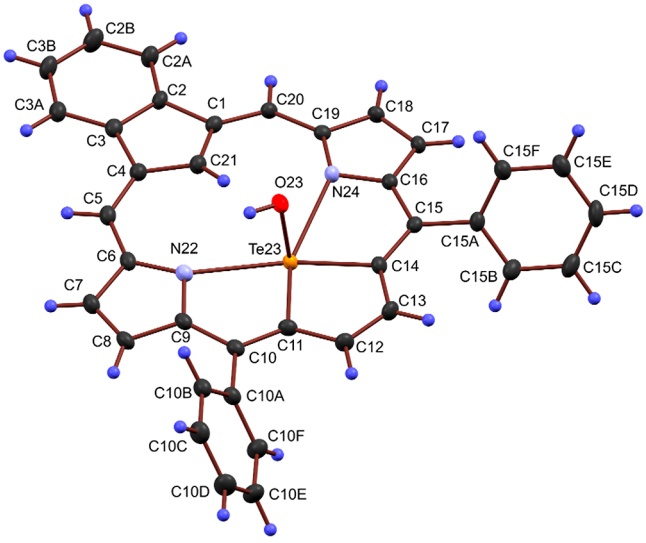

Figure 7. Color POV-Ray rendered Mercury-ORTEP III drawing (50% probability level, hydrogen atoms rendered arbitrarily small for clarity) of hydroxytelluracarbaporphyrin **19**.

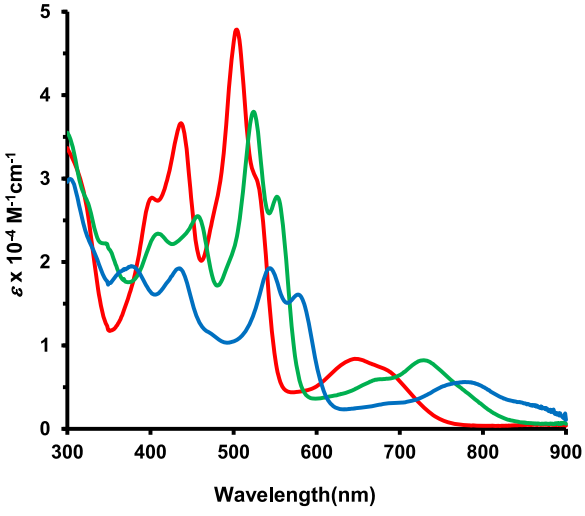

Figure 8. UV−vis spectra of palladium(II) complexes **17b** (red line), **17c** (green line), and **17d** (blue line).

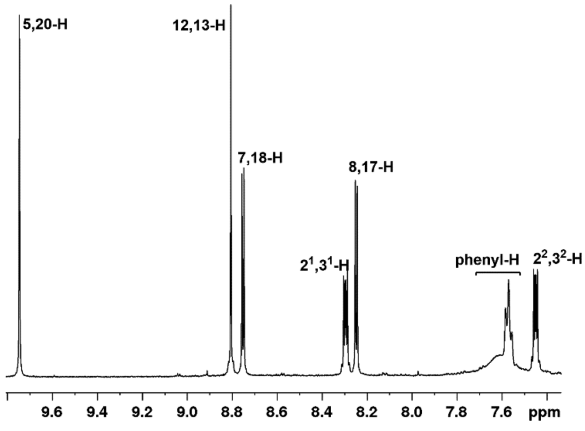

Figure 9. Proton NMR spectrum of palladium complex **17d** in $CDCl_3$ at 55 °C.

examples (74 structures) in the Cambridge Structural Database (v 5.42) containing an $R_2Te{-}PdL_3$ fragment indicate the typical palladium(II) to tellurium bonding distance is 2.54(4) Å; thus, the Pd−Te distance in this palladated tellurophene appears to be within the normal range. As for selenium analogue **17c**, the large Te atom forces the tellurophene ring to substantially rotate, by 49.2(1)°, relative to a reference plane defined by the 19 framework carbon atoms C1−C11 and C14−C21. However, this is much larger than the 36.0° rotation of the selenophene ring observed for **17c**, and the increased distortion may be responsible for the broadened electronic absorption spectrum and reduced diatropic ring current observed for **17d**. The pyrrole to reference plane ring tilts are 3.4(2) and 6.2(2)°, and the indene to reference plane tilt is 3.9(1)°. The tellurophene ring cant places the tellurium atom 0.6513(4) Å away from the Pd1,C21,N22,N24 plane and gives rise to the nonlinear 165.4(1)° C21−Pd1−Te23 bond

https://doi.org/10.1021/acs.inorgchem.1c01039
Inorg. Chem. 2021, 60, 9833−9847

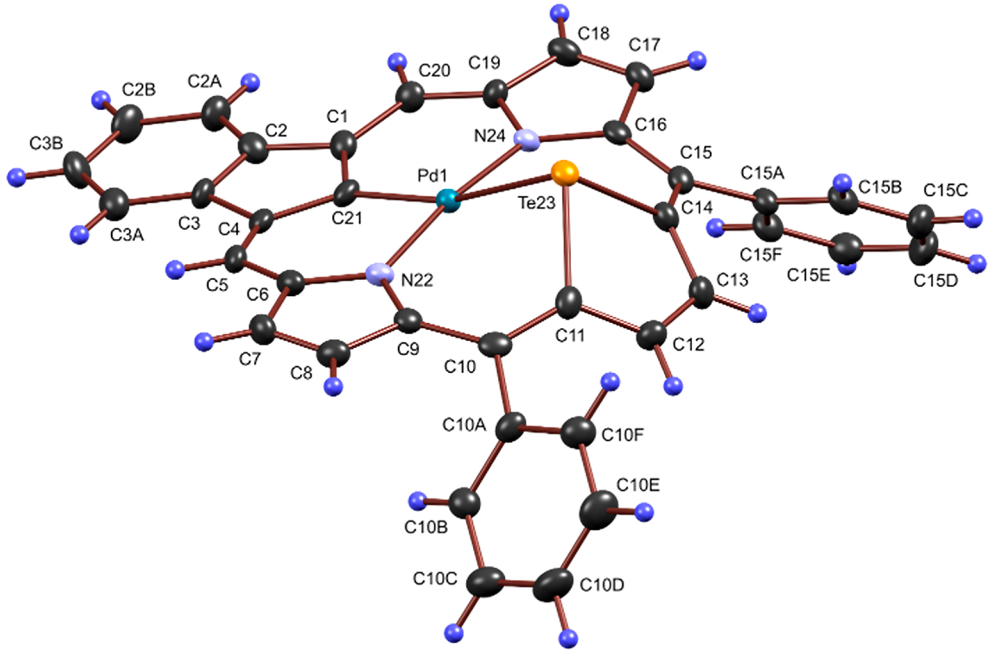

Figure 10. Color POV-Ray rendered Mercury-ORTEP III drawing (50% probability level, hydrogen atoms rendered arbitrarily small for clarity) of palladium complex **17d**.

angle. The 92.1(3)° (C21−Pd1−N22), 91.5(3)° (C21−Pd1−N24), and 173.0(2)° (N22−Pd1−N24) bond angles are all more typical for four-coordinate palladium(II). The distended 1.486(9) Å (C1−C2) and 1.480(9) Å (C3−C4) bond lengths again indicate that the π system for the benzo unit is isolated from the main macrocyclic π system. A Mogul geometry check validated all bond distances, apart from the unique Pd−Te bond (no hits), to be within typical ranges.[23]

Tellurophene dicarbinol **13d** was also reacted with oxacarbatripyrrin **9b** in the presence of boron trifluoride etherate, followed by oxidation with DDQ (Scheme 2). Although the resulting telluraoxacarbaporphyrin **15d** was only isolated in 4.9% yield, the new system proved to be stable and was not prone to air oxidation. This structure has four different elements within the porphyrinoid core and is only the third example of this type to be reported.[18] The UV−vis spectrum of **15d** was broadened and distorted in comparison to oxathiacarbaporphyrin **15b** and oxaselenacarbaporphyrin **15c** (Figure 11). Nevertheless, a weakened Soret band was present at 440 nm, and Q bands could be identified at 657 and 717 nm. Addition of TFA afforded the protonated species **15d**H^+, and this gave rise to two Soret-like bands at 443 and 514 nm, together with a broad absorption at 796 nm (Figure 12). Interestingly, the proton NMR spectrum of **15d** in $CDCl_3$ (Figure 13) indicated that the oxatelluracarbaporphyrin had a diamagnetic ring current equally strong as those of **15a−c** (Table 1). The *meso* protons (5,20-H) gave two 1H singlets at 10.24 and 10.20 ppm, while the tellurophene protons afforded two 2H doublets at 10.25 and 10.13 ppm, and the furan and pyrrole protons appeared as four 1H doublets at 9.48, 9.11, 9.07, and 8.68 ppm. The assignments for the *meso* protons were ambiguous. The peak at 10.24 ppm gave an NOE correlation with a doublet at 9.48 ppm, while irradiation of the resonance at 10.20 ppm enhanced the doublet at 9.07 ppm. Hence, assignment of the *meso* protons would in turn allow the protons on the furan and pyrrole rings to be identified. In order to address this problem, deuterated furfural **21** was

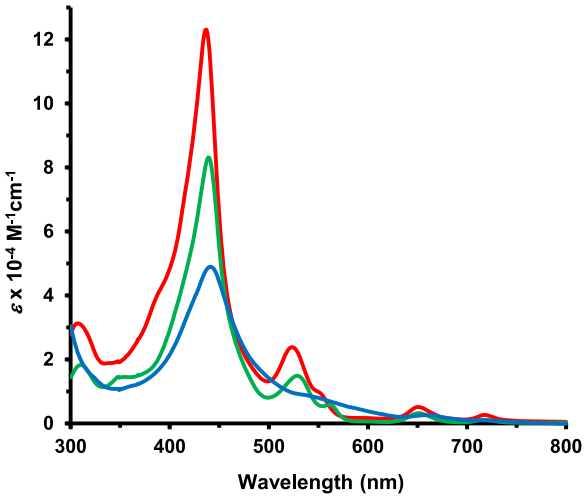

Figure 11. UV−vis spectra of oxathiacarbaporphyrin **15b** (red line), oxaselenacarbaporphyrin **15c** (green line), and oxatelluracarbaporphyrin **15d** (blue line).

reacted with dihydrofulvene **11** and KOH in refluxing ethanol for 10 min (Scheme 6). The oxacarbatripyrrin product **9b**^{D} proved to be only partially deuterated (ca. 60%), and the loss of deuterium was attributed to tautomer **22** being present at low concentrations. The reaction of **9b**^{D} with dicarbinol **13d** in the presence of boron trifluoride etherate, followed by oxidation with DDQ, gave the labeled oxatelluracarbaporphyrin **15d**^{D}. No further loss of label was observed under these reaction conditions. As the singlet at 10.24 ppm was reduced in intensity, this resonance was assigned to *meso* proton 5-H, and the doublet at 9.48 ppm therefore corresponded to furan proton 7-H. The carbon-13 NMR spectrum showed the internal CH at 125.6 pm, while the bridging methine protons appeared at 116.0 (20-CH) and 105.3 (5-CH) ppm. The last two assignments relied on a labeling study together with the

https://doi.org/10.1021/acs.inorgchem.1c01039
Inorg. Chem. 2021, 60, 9833−9847

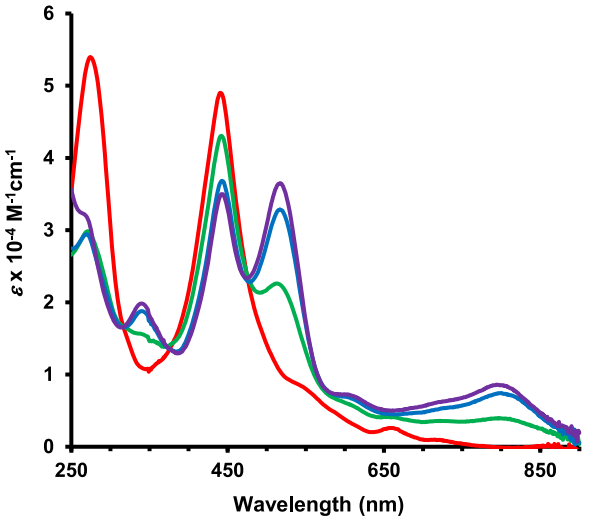

Figure 12. UV−vis spectra of oxatelluracarbaporphyrin **15d** in chloroform (red line), 0.05% TFA−99.95% chloroform (green line), 0.1% TFA−99.9% chloroform (blue line), and 0.5% TFA−99.5% chloroform (purple line) showing the gradual formation of monocation **15d**H$^+$.

HSQC spectrum. Additional support for the structure of **15d** was obtained by TOF ESI HR-MS.

COMPUTATIONAL STUDIES

In order to gain a deeper understanding of the bonding, conformations, and aromatic characteristics of these heterocarbaporphyrins, DFT studies were conducted. A series of unsubstituted heterocarbaporphyrins, **23a−d** and **24a−d**, were considered with furan, thiophene, selenophene, and tellurophene subunits (Figure 14). In addition, the related diphenyl-substituted porphyrinoids **14a−d** and **15a−d** were also investigated. Geometry optimization was performed using M06-2X with a 6-31+G** basis set. Se and Te were both modeled using the LANL2DZ basis set. Full details of these methods appear in the Experimental Section, and the complete results are disclosed in the Supporting Information. The tellurophene systems are primarily emphasized here. It was anticipated that 23-telluracarbaporphyrin **23d** would be highly distorted due to the presence of the large tellurium atom. When the dihedral angles between rings *a*, *b*, *c*, and *d* are considered, it is evident that **23d** shows the greatest divergence

Scheme 6. Synthesis of a Partially Deuterated Oxacarbaporphyrin

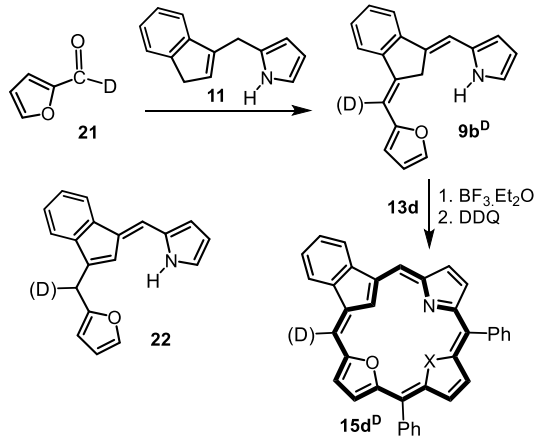

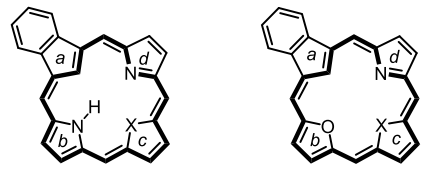

Figure 14. Unsubstituted heterocarbaporphyrins.

from planarity, followed by **23c** and **23b** (Table 2). Oxacarbaporphyrin **23a** shows the smallest amount of distortion, although significant ring tilts are still present. It was particularly noteworthy that the tellurophene unit (ring *c*) in **23d** is virtually coplanar with the adjacent pyrrolenine ring (*d*) and that it is the pyrrole and indene rings that are canted away from the mean ring plane (Figure 15). Diphenylporphyrinoids **14a−d** show similar trends. Analyses of the bond lengths in **23d** are consistent with an aromatic system, and the C−Te bond lengths were very similar to the value 2.046 Å that was reported[24] for tellurophene itself (Figure 16). However, the short distance (2.391 Å) between the tellurium and ring *d* nitrogen indicates that a covalent interaction is involved. The calculated Te−N distance for the diphenyl version **14d** was 2.397 Å (Figure 17). This type of interaction explains why rings *c* and *d* are virtually coplanar in these structures. Covalent

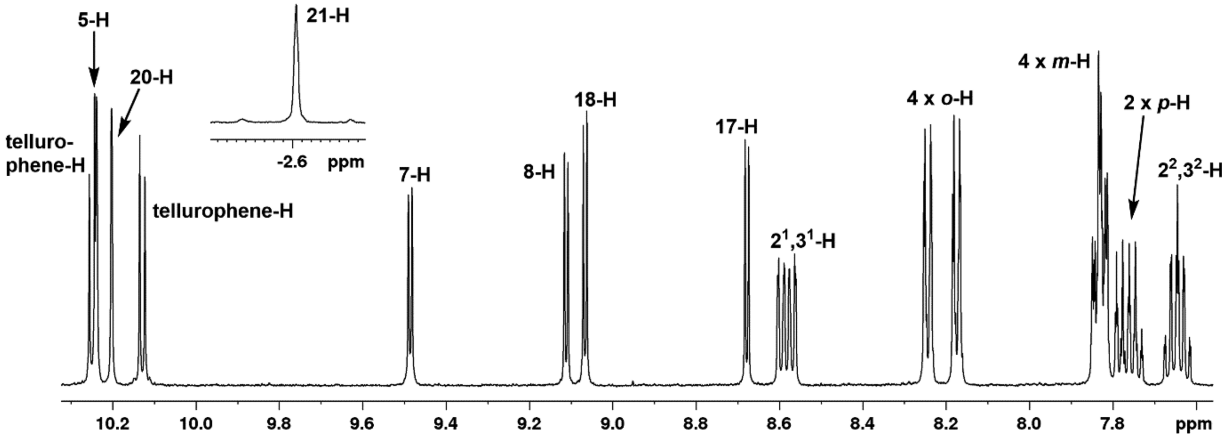

Figure 13. Proton NMR spectrum of oxatelluracarbaporphyrin **15d** in $CDCl_3$.

https://doi.org/10.1021/acs.inorgchem.1c01039
Inorg. Chem. 2021, 60, 9833−9847

Table 2. Calculated Dihedral Angles (deg) for Heterocarbaporphyrins 23a−d and 24a−d

molecule	dihedral *ab*	dihedral *bc*	dihedral *cd*	dihedral *da*	av dihedral
23a	5.66	−0.26	1.98	−7.46	3.84
23b	4.12	−1.41	9.27	−12.69	6.87
23c	4.74	−2.07	13.93	−17.28	9.51
23d	−12.38	1.70	−19.20	28.39	15.42
24a	0.00	0.00	0.00	0.00	0.00
24b	0.00	0.00	0.00	0.00	0.00
24c	0.00	0.00	0.00	0.00	0.00
24d	−16.33	0.60	−1.23	15.16	8.33
23aH^+	16.97	−5.35	5.36	−16.98	11.17
23bH^+	−17.77	15.52	−15.54	17.79	16.66
23cH^+	−16.55	25.36	−25.34	16.52	20.94
23dH^+	−14.63	32.97	−34.77	14.64	24.25
24aH^+	10.42	−3.99	0.65	−7.28	5.59
24bH^+	−16.31	11.86	−3.29	6.71	9.54
24cH^+	−17.09	19.76	−9.34	5.43	12.91
24dH^+	12.29	−32.62	22.97	−1.79	17.42

interactions of this type have previously been proposed for heterotelluraporphyrins such as **3**,[5] and hypervalent tellurium species have been well documented in the literature.[25]

Protonation of these structures to give the related cations **14**H^+ and **23**H^+ considerably alters the conformations of these structures. Protonation of the nitrogen prevents covalent interactions with the tellurium atom in **23d**H^+, and for this reason the tellurophene ring is no longer held within the macrocyclic plane (Figure 18) and the dihedral angles between all of the subunits are greatly increased. Distortions to the macrocycle are seen in **23a−c** due to increased crowding within the porphyrinoid cavity, and these increase in direct response to the size of the heteroatom. Protonated diphenylheterocarbaporphyrinoids **14a−d** showed similar effects.

22-Oxaheterocarbaporphyrins **24a−d** and their diphenyl congeners **15a−d** were also examined. The conformations of **24a−c** are planar (Table 2), although the related diphenylporphyrinoids **15a−c** show significant divergence from planarity. For the unsubstituted series **24a−d**, only oxatelluracarbaporphyrin **24d** is significantly distorted (Figure 15), and this is further exacerbated for the diphenyl version **15d**. Importantly, it is the indene moiety that is pivoted from the macrocyclic plane and the tellurophene unit is essentially coplanar with the furan and pyrrole rings in both **15d** and **24d**. The distances between the tellurium and nitrogen atoms are 2.455 Å in **24d** and 2.462 Å in **15d** (Figures 16 and 17), implying that these atoms are connected by a covalent bond. The Te−O internuclear distances for **24d** and **15d** are 2.743 and 2.739 Å, respectively, suggesting that there is also a weaker covalent interaction between these atoms as well. Therefore, hypervalent tellurium interactions appear to substantially affect the conformations of telluracarbaporphyrins and oxatelluracarbaporphyrins. The rest of the macrocycle's bond lengths are consistent with an aromatic system where the π system of the benzo unit is disconnected from the 18-π-electron delocalization pathway. Protonation of these porphyrinoids leads to further distortions. In cations **15d**H^+ and **24d**H^+, the tellurophene unit is pivoted away from the rest of the macrocycle (Figure 18) as there can no longer be any covalent interactions between the tellurium and the other heteroatoms.

The aromatic characters of heterocarbaporphyrins were assessed using nuclear independent chemical shift (NICS) calculations[26] and anisotropy of induced current density (AICD) plots,[27] methods we have previously applied to related porphyrinoid systems.[28−32] NICS(0) calculations are commonly used to identify the aromatic characteristics of porphyrinoid systems, but the results can be misleading, as the effects of both the σ and π electrons are included. $NICS_{zz}$ calculations carried out 1 Å above the ring ($NICS(1)_{zz}$) emphasize contributions from the π system, and this method is a more reliable indicator of macrocyclic diatropicity. In this work, both NICS and $NICS_{zz}$ results were calculated. Both methods demonstrated that 23-heterocarbaporphyrins **23a−d** possess strongly diatropic properties (Table 3). The $NICS(1)_{zz}$ values indicate that telluracarbaporphyrin **23d** has a slightly reduced diatropic ring current, although this is not mirrored in the NICS(0) calculations. The NICS(0) and $NICS(1)_{zz}$ values for the individual rings in **23a−d** show large negative values for pyrrole ring *d* and furan ring *c*, but pyrrolenine ring *b* gave greatly reduced negative values and ring *a* afforded a positive result. These data indicate that an 18-π-electron delocalization pathway is favored that passes around the outside of rings *c* and *d* but primarily runs through the interior of ring *b* and exclusively goes through the inside portion of the indene ring (Table 3). The benzo units (ring *e*) behave like isolated benzene rings. The results for heterooxacarbaporphyrins **24a−d** indicate that a similar 18-π-electron circuit is present that passes inside rings *a* and *b* and on the outside of rings *c* and *d* (Table 4). The corresponding diphenylporphyrinoids **14a−d** and **15a−d** showed comparable results.

The NICS(0) and $NICS(1)_{zz}$ results for dications **23a−d**H^+ and **24a−d**H^+ showed that a rather different conjugation pathway was present (Tables 3 and 4). The macrocycles retained strongly aromatic characteristics, but the NICS(0)

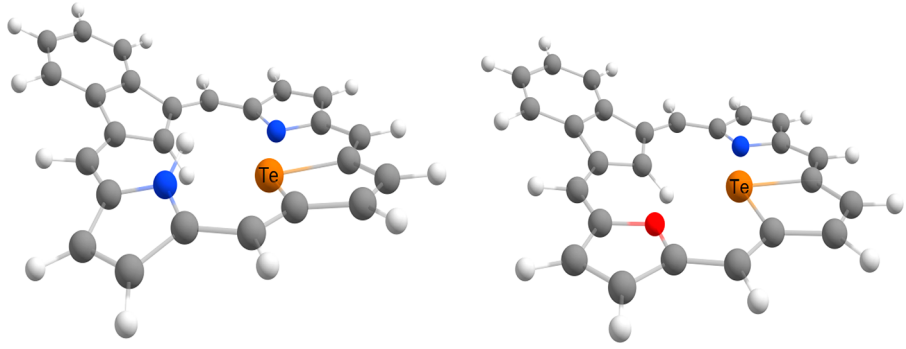

Figure 15. Conformations of telluracarbaporphyrin **23d** (right) and oxatelluracarbaporphyrin **24d** (left).

https://doi.org/10.1021/acs.inorgchem.1c01039
Inorg. Chem. 2021, 60, 9833−9847

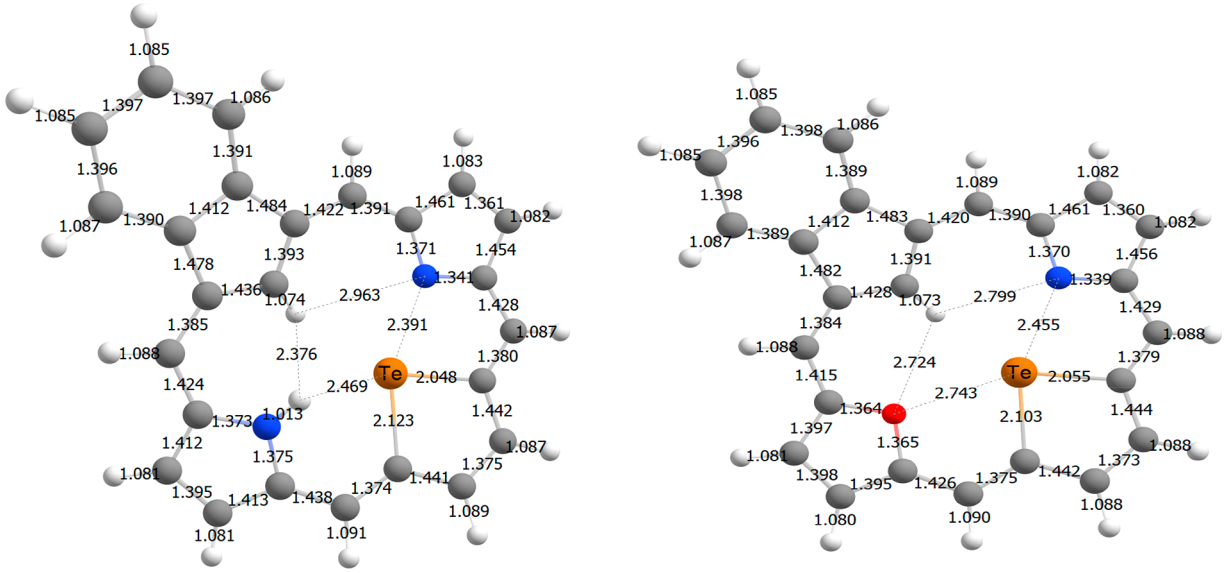

Figure 16. Calculated bond lengths for telluracarbaporphyrin **23d** (right) and oxatelluracarbaporphyrin **24d** (left).

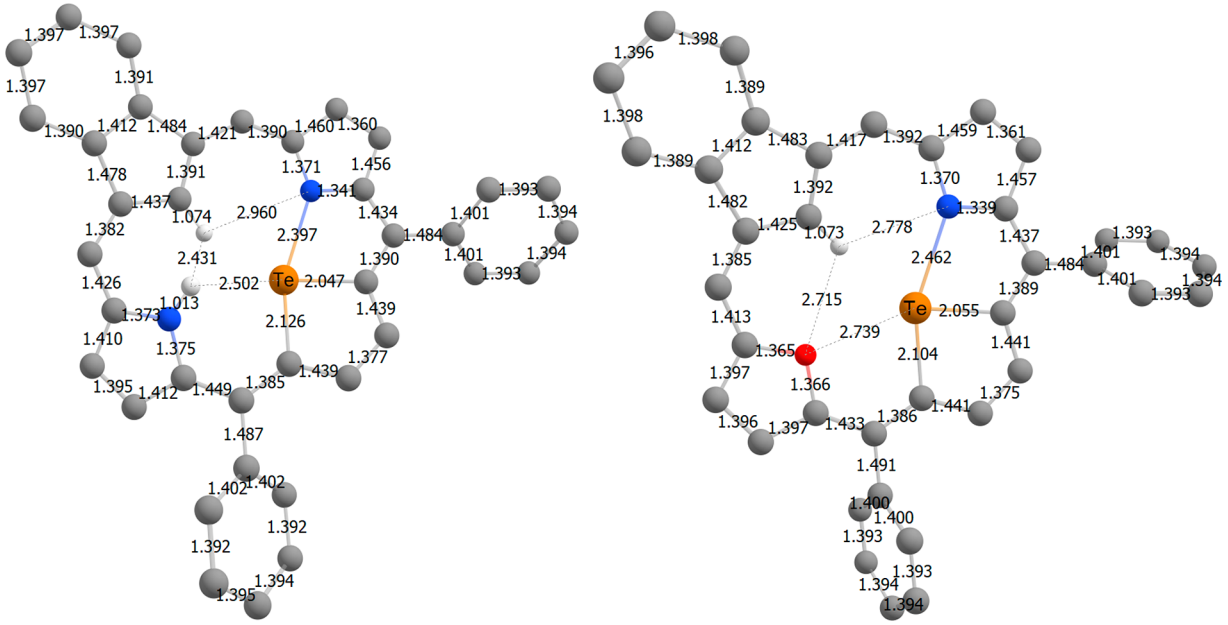

Figure 17. Calculated bond lengths for diphenyltelluracarbaporphyrin **14d** (right) and oxatelluracarbaporphyrin **15d** (left).

and $NICS(1)_{zz}$ values were both diminished for the telluracarbaporphyrin cations **23d**H^+ and **24d**H^+. When the values for the individual rings were considered, it was apparent that the favored aromatic pathway extended around the outside of rings *b*−*d* and only passed through the inside of ring *a*. The pathway is best considered to be a 19-atom 18-π-electron circuit as shown in Figure 19. Similar results were obtained for diphenylcarbaporphyrinoid cations **14a**−**d**H^+ and **15a**−**d**H^+.

AICD plots were obtained for all of these structures. Free base telluracarbaporphyrin **23d** and telluracarbaporphyrin **24d** are shown in Figure 20, and these results are consistent with the proposed delocalization pathways. Furthermore, the AICD plots for cations **23d**H^+ and **24d**H^+ clearly show the delocalization pathway extending around rings *b*−*d* (Figure 21). It is also clear from these figures that the benzo units are not significantly interacting with the rest of the π system.

The oxidation products derived from telluracarbaporphyrins were also investigated. The energies (ΔG) for hydroxytelluracarbaporphyrins and the tautomeric tellurophene oxides were contrasted, and as expected the hydroxytelluracarbaporphyrins were favored. When the unsubstituted hydroxytellurophene porphyrinoid **25** was considered, two conformational minima (A and B) could be detected for the corresponding tellurophene oxides **26** (Table 5). The more stable of these conformations was still 12.29 kcal/mol higher in energy than the hydroxy tautomer. Although a similar trend can be observed for the diphenyl congeners **19** and **20**, some important differences emerged between the substituted and unsubstituted structures. Unsubstituted hydroxy tautomer **25** pivots the OH group away from the macrocyclic cavity and shows little sign of covalent interactions between the nitrogens and the tellurium atom. However, the calculated conformational minimum for diphenyl congener **19** has the OH oriented

https://doi.org/10.1021/acs.inorgchem.1c01039
Inorg. Chem. 2021, 60, 9833−9847

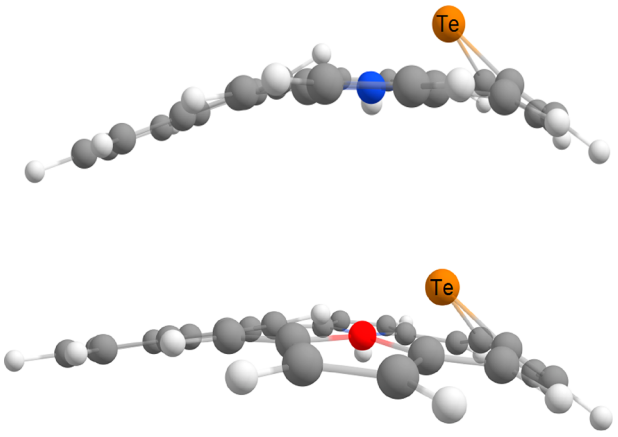

Figure 18. Conformations of monoprotonated telluraporphyrinoids **23d**H$^+$ (top) and **24d**H$^+$ (bottom).

into the cavity and has short N−Te separations, in agreement with the X-ray crystal structure. Notably, this leads to a much larger difference in the energies where **19** is favored over **20** (again there are two conformational minima) by ca. 30 kcal/mol (Table 5).

NICS(0) and NICS(1)$_{zz}$ calculations for hydroxytelluracarbaporphyrins and the related tellurophene oxides indicate that the aromatic ring currents are diminished, particularly in the unsubstituted series (Table 6). Diphenyl hydroxytelluracarbaporphyrin **19** gave the largest negative NICS(1)$_{zz}$ value of −20.18 ppm. An analysis of the values for the rings *a*−*d* indicates that the dominant circuit involves an anionic 17-atom 18-π-electron pathway (Figure 19). AICD plots for **19** and **25** were also consistent with this supposition (Figure 22). On the other hand, oxides **20A,B** and **26A,B** favor a more conventional 18-atom pathway that passes through the inside of rings *a* and *b* and the outside of rings *c* and *d*.

CONCLUSIONS

The first examples of telluracarbaporphyrins have been synthesized. A diphenyltelluracarbaporphyrin with a CNTeN core proved to be very sensitive to air oxidation and afforded a related hydroxytelluracarbaporphyrin. However, an oxatelluraporphyrin with a CNTeO core did not undergo oxidations of this kind. All three structures, including the hydroxytellurophene system, exhibited strongly diatropic characteristics, although their UV−vis spectra were broadened and bathochromically shifted compared to other heterocarbaporphyrins. The tellurium atom in these macrocycles appears to be involved in hypervalent interactions with core nitrogen atoms. This was supported by the X-ray crystal structure for the oxidation product, as well as by DFT studies. Diphenyltelluracarbaporphyrin also reacted with palladium(II) acetate to give an organometallic derivative where the palladium cation is coordinated to all four atoms in the CNTeN core. The results show that tellurium-containing porphyrinoids have unusual and intriguing characteristics, while demonstrating useful trends in heterocarbaporphyrin systems.

EXPERIMENTAL SECTION

Melting points are uncorrected. NMR spectra were recorded using a 400 or 500 MHz NMR spectrometer and were run at 302 K unless otherwise indicated. ^{1}H NMR values are reported as chemical shifts δ, relative integral, multiplicity (s, singlet; d, doublet; t, triplet; q, quartet; m, multiplet; br, broad peak), and coupling constant (*J*). Chemical shifts are reported in parts per million (ppm) relative to $CDCl_3$ (^{1}H residual $CHCl_3$ singlet δ 7.26, ^{13}C $CDCl_3$ triplet δ 77.23),

Table 3. NICS(0) and NICS(1)$_{zz}$ Values (ppm) for Unsubstituted Heterocarbaporphyrins 23a−d and 24a−d

	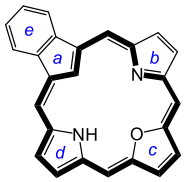 **23a**	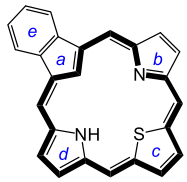 **23b**	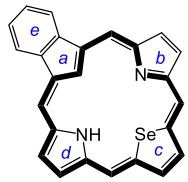 **23c**	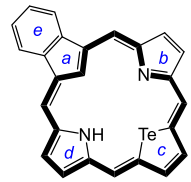 **23d**
NICS(0) | NICS(01)$_{zz}$	−12.83 | −32.47	−13.57 | −32.67	−13.21 | −29.77	−14.58 | −22.58
NICS(a) | NICS(a1)$_{zz}$	+08.54 | +19.91	+07.96 | +17.66	+07.10 | +11.64	+04.98 | +15.34
NICS(b) | NICS(b1)$_{zz}$	−01.69 | −11.98	−01.71 | −11.14	−01.92 | −14.06	−03.77 | −12.14
NICS(c) | NICS(c1)$_{zz}$	−15.63 | −38.64	−15.57 | −32.16	−14.04 | −36.37	−10.80 | −15.57
NICS(d) | NICS(d1)$_{zz}$	−14.23 | −37.17	−14.74 | −42.66	−14.90 | −27.94	−14.45 | −40.65
NICS(e) | NICS(e1)$_{zz}$	−04.65 | −17.04	−04.87 | −17.78	−05.18 | −19.71	−05.78 | −17.22
	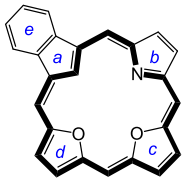 **24a**	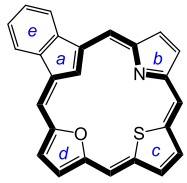 **24b**	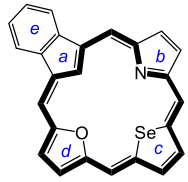 **24c**	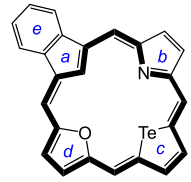 **24d**
NICS(0) | NICS(01)$_{zz}$	−13.52 | −34.20	−14.72 | −34.96	−14.81 | −32.10	−16.05 | −31.93
NICS(a) | NICS(a1)$_{zz}$	+10.93 | +22.47	+10.51 | +21.31	+09.72 | +19.32	+06.55 | +10.45
NICS(b) | NICS(b1)$_{zz}$	−00.69 | −09.85	−01.33 | −11.01	−01.67 | −11.78	−03.05 | −14.83
NICS(c) | NICS(c1)$_{zz}$	−15.73 | −41.09	−15.60 | −36.20	−13.80 | −30.79	−10.02 | −26.50
NICS(d) | NICS(d1)$_{zz}$	−16.94 | −43.29	−17.27 | −43.75	−17.32 | −43.49	−16.63 | −41.99
NICS(e) | NICS(e1)$_{zz}$	−03.93 | −16.18	−04.08 | −16.58	−04.35 | −17.35	−05.23 | −19.11

https://doi.org/10.1021/acs.inorgchem.1c01039
Inorg. Chem. 2021, 60, 9833−9847

Table 4. NICS(0) and NICS(1)$_{zz}$ Values (ppm) for Unsubstituted Monoprotonated Heterocarbaporphyrins 23a−dH$^+$ and 24a−dH$^+$

	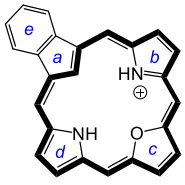 **23aH$^+$**	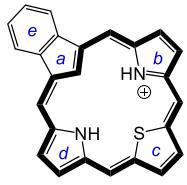 **23bH$^+$**	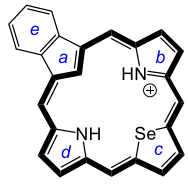 **23cH$^+$**	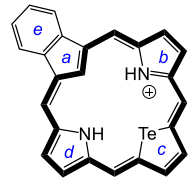 **23dH$^+$**
NICS(0) | NICS(01)$_{zz}$	−14.03 | −34.41	−14.21 | −33.49	−13.86 | −35.08	−13.20 | −26.77
NICS(a) | NICS(a1)$_{zz}$	+08.96 | +26.56	+09.85 | +26.87	+09.18 | +15.11	+08.46 | +23.27
NICS(b) | NICS(b1)$_{zz}$	−13.09 | −37.95	−13.16 | −40.49	−12.89 | −28.77	−12.54 | −34.56
NICS(c) | NICS(c1)$_{zz}$	−17.18 | −39.37	−18.15 | −30.52	−18.39 | −62.63	−18.07 | −38.29
NICS(d) | NICS(d1)$_{zz}$	−13.08 | −37.92	−13.16 | −40.50	−12.90 | −28.75	−12.54 | −34.55
NICS(e) | NICS(e1)$_{zz}$	−04.90 | −15.61	−04.64 | −15.58	−04.83 | −18.51	−05.12 | −16.91
	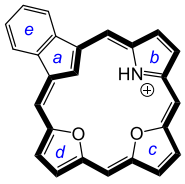 **24aH$^+$**	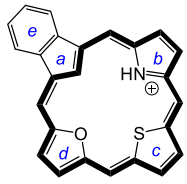 **24bH$^+$**	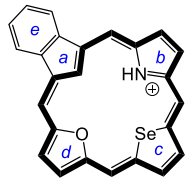 **24cH$^+$**	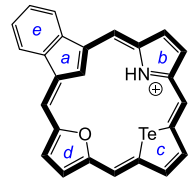 **24dH$^+$**
NICS(0) | NICS(01)$_{zz}$	−14.02 | −35.84	−14.69 | −35.06	−14.90 | −35.95	−13.98 | −28.52
NICS(a) | NICS(a1)$_{zz}$	+12.63 | +24.76	+12.67 | +30.84	+12.31 | +23.32	+11.95 | +28.30
NICS(b) | NICS(b1)$_{zz}$	−12.68 | −29.31	−13.30 | −42.13	−13.46 | −26.17	−13.02 | −37.51
NICS(c) | NICS(c1)$_{zz}$	−16.73 | −44.69	−17.26 | −34.70	−17.24 | −45.39	−17.63 | −31.51
NICS(d) | NICS(d1)$_{zz}$	−16.87 | −43.38	−16.51 | −41.71	−16.43 | −45.39	−15.91 | −35.51
NICS(e) | NICS(e1)$_{zz}$	−03.72 | −15.56	−03.69 | −14.28	−03.78 | −15.78	−04.01 | −15.43

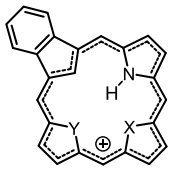

23a-dH$^+$ Y = NH
24a-dH$^+$ Y = O

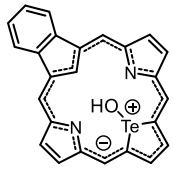

25

Figure 19. Proposed conjugation pathways in monoprotonated heterocarbaporphyrin cations **23a−dH$^+$/24a−dH$^+$** and hydroxytellur-acarbaporphyrin **25**.

and coupling constants were taken directly from the spectra. NMR assignments were made with the aid of ^{1}H−^{1}H COSY, HSQC, DEPT-135, and NOE difference proton NMR spectroscopy. 2D experiments were performed using standard software. High-resolution mass spectra (HRMS) were obtained using a double-focusing magnetic sector instrument. ^{1}H and ^{13}C NMR spectra for all new compounds are reported in the Supporting Information.

10,15-Diphenyl-23-tellurabenzo[*b*]carbaporphyrin (14d). Carbatripyrrin **9a** (50 mg, 0.184 mmol) and tellurophene dicarbinol **13d** (72.1 mg, 0.184 mmol) were stirred with dichloromethane (300 mL) and flushed with nitrogen for 10 min. A 10% boron trifluoride etherate solution in dichloromethane (125 μL) was added over several minutes, and the resulting mixture was stirred in the dark under a nitrogen atmosphere for 2 h. DDQ (83 mg, 0.366 mmol) was added, and the solution was stirred for an additional 30 min. The resulting mixture was washed with water and dried over sodium sulfate and the solvent removed under reduced pressure. The residue was purified on a grade 3 basic alumina column with dichloromethane as eluent, and a large brown band was collected. The solvent was removed under reduced pressure, and the residue was further purified on a grade 2 basic alumina column, with 2% ethyl acetate−98% toluene as eluent with a gradual increase in the polarity to 15% ethyl acetate−85% toluene. On the column, the product appeared as a green band but was collected as an orange-red solution. Evaporation of the solvent under reduced pressure gave diphenyltelluracarbapor-phyrin **14d** (31.3 mg, 0.0437 mmol, 27%) as a dark air-sensitive solid: mp >300 °C dec. UV−vis (0.335 μM **14d** in 1% Et_3N−99% CH_2Cl_2):

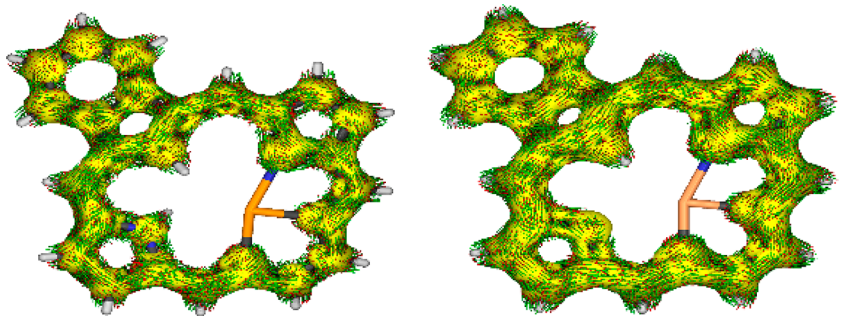

Figure 20. AICD plots (isovalue 0.05) for telluracarbaporphyrin **23d** (left) and oxacarbatelluraporphyrin **24d** (right).

https://doi.org/10.1021/acs.inorgchem.1c01039
Inorg. Chem. 2021, 60, 9833−9847

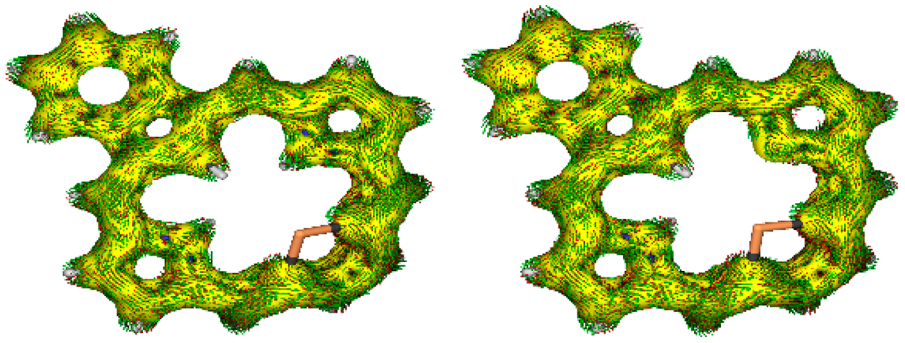

Figure 21. AICD plots (isovalue 0.05) for telluracarbaporphyrin cation **23d**H$^+$ (left) and oxacarbatelluraporphyrin **24d**H$^+$ (right).

Table 5. Calculated Relative Energies (ΔG, kcal/mol) of Hydroxytelluraporphyrins and Their Tellurophene Oxide Tautomers

	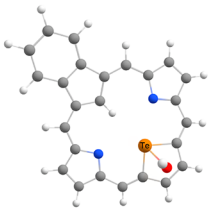 **25**	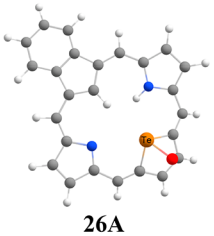 **26A**	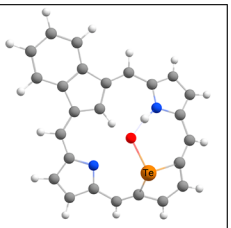 **26B**
ΔG_{298} (kcal/mol)	0.00	17.00	12.29
	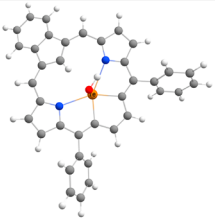 **19**	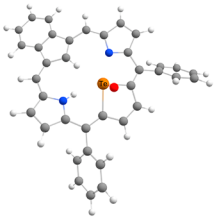 **20A**	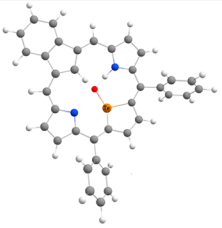 **20B**
ΔG_{298} (kcal/mol)	0.00	31.28	28.62

λ_{max} (log ε) 284 (4.48), 446 (4.85), 639 (3.83), 568 (sh, 3.99), 713 (sh, 3.57). UV−vis (0.335 μM **14d** in 0.1% TFA−99.9% CH_2Cl_2): λ_{max} (log ε) 269 (4.39), 348 (4.40), 393 (4.32), 446 (4.58), 527 (4.61), 555 (4.62), 814 (4.05). UV−vis (0.127 μM **14d** in 1% TFA−99% $CHCl_3$): λ_{max} (log ε) 272 (4.33), 304 (sh, 4.28), 324 (sh, 4.33), 348 4.36), 393 (4.30), 445 (4.58), 526 (4.63), 556 (4.65), 817 (4.10). UV−vis (0.127 μM **14d** in 10% TFA−90% $CHCl_3$): λ_{max} (log ε) 271 (4.25), 325 (4.26), 471 (5.05), 611 (sh, 4.07), 639 (4.08), 710 (sh, 3.99). ^{1}H NMR ($CDCl_3$, 500 MHz): δ 10.14 (s, 2H, 5,20-H), 9.98 (s, 2H, 12,13-H), 8.94 (d, 2H, $^3J_{HH}$ = 4.4 Hz, 7,18-H), 8.65−8.62 (m, 2H, 2^1,3^1-H), 8.60 (d, 2H, $^3J_{HH}$ = 4.3 Hz, 7,18-H), 8.27 (d, 4H, $^3J_{HH}$ = 7.5 Hz, 4 × *o*-H), 7.84 (t, 4H, $^3J_{HH}$ = 7.5 Hz, 4 × *m*-H), 7.75 (t, 2H, $^3J_{HH}$ = 7.5 Hz, 2 × *p*-H), 7.70−7.66 (m, 2H, 2^2,3^2-H), −2.21 (br s, 1H, NH), −2.58 (s, 1H, 21-H). {^{1}H}^{13}C NMR ($CDCl_3$, 125 MHz): δ 142.1, 140.6, 140.5 (12,13-CH), 136.3, 135.5, 134.6 (4 × *o*-CH), 129.0, 128.5 (4 × *m*-CH), 128.3 (2 × *p*-CH), 127.4 (2^2,3^2-CH), 126.5 (8,17-CH), 120.9 (2^1,3^1-CH), 117.9 (21-CH), 111.6 (5,20-CH). HR-MS (ESI) *m*/*z*: [M + H]$^+$ calcd for $C_{37}N_{25}N_2Te$, 627.1080; found, 627.1083.

10,15-Diphenyl-23-hydroxy-23-tellurabenzo[*b*]-carbaporphyrin (19). Carbatripyrrin **9a** (50 mg, 0.184 mmol) and tellurophene dicarbinol **13d** (72.1 mg, 0.184 mmol) were reacted under the aforementioned conditions. The crude product was shaken with a 0.1% aqueous ferric chloride solution for 5−7 min and then washed sequentially with water, 5% sodium bicarbonate, and water. Purification by column chromatography on grade 3 basic alumina with 2−5% ethyl acetate−98−95% toluene as eluent gave a green solution. Recrystallization form chloroform−methanol gave **19** (29.7 mg, 0.0462 mmol, 25%) as a dark solid: mp >300 °C. UV−vis (0.124 μM **19** in $CHCl_3$): λ_{max} (log ε) 313 (4.51), 353 (sh, 4.22), 470 (4.89), 516 (4.45), 612 (sh, 3.74), 648 (sh, 3.80), 715 (4.32). UV−vis (0.124 μM **19** in 0.05% TFA−99.95% $CHCl_3$): λ_{max} (log ε) 268 (4.47), 330 (4.45), 474 (4.93), 548 (4.34), 684 (sh, 3.92), 752 (4.30). UV−vis (0.124 μM **19** in 10% TFA−90% $CHCl_3$): λ_{max} (log ε) 476 (4.95), 642 (4.08). ^{1}H NMR ($CDCl_3$, 500 MHz): δ 10.33 (s, 2H, 5,20-H), 9.97 (s, 2H, 12,13-H), 8.94 (d, 2H, $^3J_{HH}$ = 4.1 Hz, 7,18-H), 8.51−8.49 (m, 2H, 2^1,3^1-H), 8.49 (d, 2H, $^3J_{HH}$ = 4.1 Hz, 7,18-H), 8.20 (br d, 4H, 4 × *o*-H), 7.84 (t, 4H, $^3J_{HH}$ = 7.5 Hz, 4 × *m*-H), 7.76 (t, 2H, $^3J_{HH}$ = 7.5 Hz. Two × *p*-H), 7.62−7.59 (m, 2H, 2^2,3^2-H), −2.06 (s, 1H, 21-H), −3.82 (s, 1H, OH). {^{1}H}^{13}C NMR ($CDCl_3$, 50 °C, 125 MHz): δ 154.3, 147,5. 140.8, 139.1, 137.7, 137.0, 135.7 (7,18-C), 135.6 (12,13-CH), 133.0 (4 × *o*-CH), 128.7 (4 × *m*-CH), 128.5 (2 × *p*-CH), 127.2 (21-CH), 126.5 (2^2,3^2-CH), 126.2 (8,17-CH), 120.1 (2^1,3^1-CH), 118.8 (5,20-CH). HR-MS (ESI) *m*/*z*: M$^+$ calcd for $C_{37}N_{24}N_2OTe$, 642.0951; found, 642.0970.

10,15-Diphenyl-22-oxa-23-tellura-21-carbabenzo[*b*]-porphyrin (15d). Oxacarbatripyrrin **9b** (50.2 mg, 0.0184 mmol) and tellurophene dicarbinol **13d** (72.1 mg, 0.0184 mmol) were dissolved in dichloromethane (300 mL) under nitrogen and stirred for several minutes. A 10% solution of BF_3·Et_2O in dichloromethane (125 μL) was added dropwise over 5 min. The mixture was then stirred under nitrogen for 2 h. DDQ (83 mg) was added and the mixture stirred for an additional 30 min. The solution was then washed with water and dried over sodium sulfate and the solvent evaporated. The residue was purified by column chromatography on grade 2 basic alumina with dichloromethane as eluent and rechromatographed on grade 2 basic alumina with 2:1 hexanes−dichloromethane as eluent. Evaporation of the solvent gave the oxatelluracarbaporphyrin (5.6 mg, 8.96 μmol,

https://doi.org/10.1021/acs.inorgchem.1c01039
Inorg. Chem. 2021, 60, 9833−9847

Table 6. Calculated NICS(0) and NICS(1)$_{zz}$ Values (ppm) for Hydroxytelluraporphyrins and Their Tellurophene Oxide Tautomers

	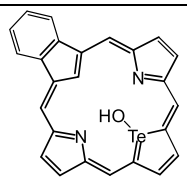 **25**	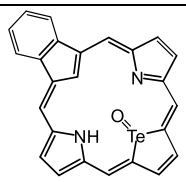 **26A**	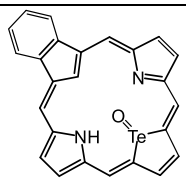 **26B**
NICS(0) | NICS(1)$_{zz}$	−06.95 | −14.41	−04.28 | −06.30	−08.74 | −11.58
NICS(a) | NICS(a)$_{zz}$	+02.70 | +03.13	+02.97 | +03.74	+04.97 | +07.67
NICS(b) | NICS(b)$_{zz}$	−04.54 | −15.74	−00.77 | −09.80	−02.10 | −13.82
NICS(c) | NICS(c)$_{zz}$	−13.86 | −38.16	−06.23 | −33.51	−09.32 | −35.24
NICS(d) | NICS(d)$_{zz}$	−04.54 | −15.74	−11.93 | −24.09	−11.59 | −32.29
NICS(e) | NICS(e)$_{zz}$	−06.52 | −22.84	−06.76 | −23.19	−06.10 | −20.19
	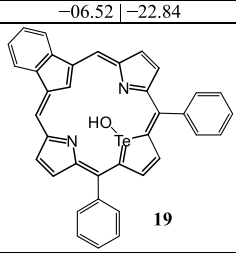 **19**	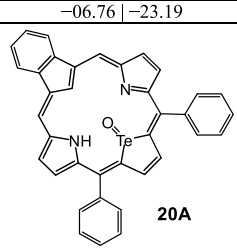 **20A**	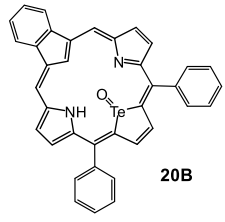 **20B**
NICS(0) | NICS(1)$_{zz}$	−13.33 | −20.18	−05.58 | −09.80	−10.44 | −14.49
NICS(a) | NICS(a)$_{zz}$	+03.51 | +08.48	+03.79 | +05.49	+05.87 | +09.89
NICS(b) | NICS(b)$_{zz}$	−06.64 | −20.71	−00.83 | −08.20	−02.00 | −11.11
NICS(c) | NICS(c)$_{zz}$	−13.44 | −32.85	−06.44 | −35.47	−09.59 | −35.16
NICS(d) | NICS(d)$_{zz}$	−05.94 | −19.82	−12.35 | −23.18	−11.44 | −31.70
NICS(e) | NICS(e)$_{zz}$	−06.22 | −18.27	−06.44 | −22.63	−05.70 | −20.47

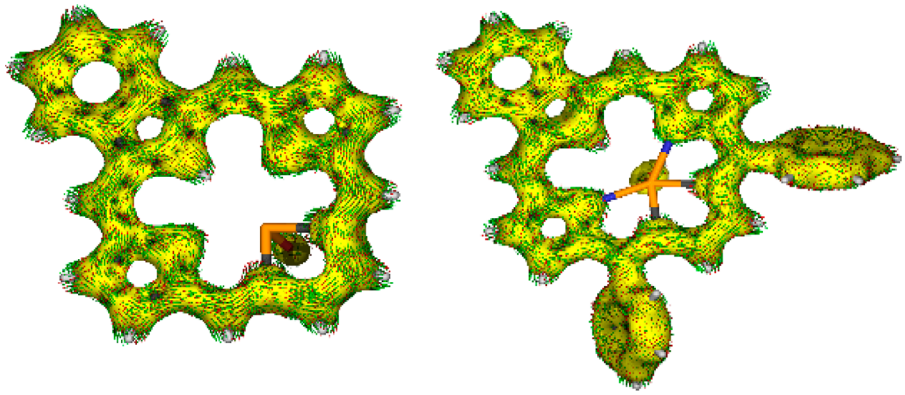

Figure 22. AICD plots (isovalue 0.05) of hydroxytelluracarbaporphyrin **25** and its diphenyl congener **19**.

4.9%) as a brown solid. UV−vis (0.144 μM **15d** in CH_2Cl_2): λ_{max} (log ε) 278 (4.34), 315 (sh, 4.14), 440 (4.72), 537 (sh, 3.88), 657 (3.36), 717 (2.87). UV−vis (0.144 μM **15d** in 0.1% TFA−99.9% CH_2Cl_2): λ_{max} (log ε) 270 (4.29), 339 (4.24), 443 (4.56), 514 (4.60), 796 (3.91). UV−vis (0.144 μM **15d** in 50% TFA−50% CH_2Cl_2): λ_{max} (log ε) 258 (4.xx), 274, 335, 447, 482, 724. ^{1}H NMR ($CDCl_3$, 500 MHz): δ 10.25 (d, 1H, $^3J_{HH}$ = 6.2 Hz, 12- or 13-H), 10.24 (s, 1H, 5-H), 10.20 (br s, 1H, 20-H), 10.13 (d, 1H, $^3J_{HH}$ = 6.2 Hz, 12- or 13-H), 9.48 (d, 1H, $^3J_{HH}$ = 4.3 Hz, 7-H), 9.11 (d, 1H, $^3J_{HH}$ = 4.3 Hz, 8-H), 9.07 (d, 1H, $^3J_{HH}$ = 4.3 Hz, 18-H), 8.68 (d, 1H, $^3J_{HH}$ = 4.3 Hz, 17-H), 8.60−8.56 (m, 2H, 2^1,3^1-H), 8.26−8.23 (m, 4H, 4 × *o*-H), 7.85−7.81 (m, 4H, 4 × *m*-H), 7.79−7.73 (m, 2H, 2 × *p*-H), 7.68−7.61 (m, 2H, 2^2,3^2-H), −2.58 (br t, 1H, 21-H). {^{1}H}^{13}C NMR ($CDCl_3$, 125 MHz): δ 158.0, 156.5, 156.3, 152.1, 151.8, 144.6, 142.5, 142.3 (12- or 13-CH), 141.5, 140.5 (12- or 13-CH), 140.1, 139.6, 137.3, 136.0 (18-CH), 135.2, 134.2, 133.5, 132.1, 130.9 (17-CH), 128.5, 128.4, 127.9, 127.3 (2^2,3^2-CH), 125.8 (7-CH), 125.6 (21-CH), 123.3 (8-CH), 121.0, 120.8 (2^1,3^1-CH), 116.0 (20-CH), 105.3 (5-CH). ^{1}H NMR (TFA−$CDCl_3$, 500 MHz): δ 9.99 (s, 1H), 9.88 (s, 1H) (5,20-H), 9.63 (d, 1H, $^3J_{HH}$ = 4.6 Hz), 9.38 (d, 1H, $^3J_{HH}$ = 4.6 Hz), 9.16 (d, 1H, $^3J_{HH}$ = 5.4 Hz), 9.09 (d, 1H, $^3J_{HH}$ = 4.5 Hz), 8.90 (d, 1H, $^3J_{HH}$ = 4.5 Hz), 8.85 (d, 1H, $^3J_{HH}$ = 5.4 Hz), 8.42−8.39 (m, 4H), 8.22−8.20 (m, 2H), 7.85−7.81 (m, 4H, 4 × *m*-H), 7.97 (t, 2H, $^3J_{HH}$ = 7.4 Hz, 2 × *p*-H), 7.91−7.84 (m, 4H), 7.60 (m, 2H), −3.43 (s, 1H). HR-MS (ESI) *m*/*z*: [M + H]$^+$ calcd for $C_{37}H_{24}NOTe$, 628.0920; found, 628.0942.

(10,15-Diphenyl-23-oxa-21-carbabenzo[b]porphyrinato)-palladium(II) (17d). Crude telluracarbaporphyrin **19**, prior to chromatography, obtained by reacting **9a** (50.0 mg, 0.184 mmol) and **13d** (72.1 mg, 0.184 mmol) under the conditions described above, was dissolved in 50:50 chloroform−acetonitrile (25 mL) and stirred at room temperature under nitrogen with palladium(II) acetate (25 mg) for 30 min. The solvent was evaporated under reduced pressure and the residue purified by column chromatography on grade 2 alumina, with 50% dichloromethane−50% hexanes as eluent, to give a deep red fraction. Evaporation of the solvent gave the palladium complex (21.3 mg, 0.0292 mmol, 16%) as a red solid: mp >300 °C. UV−vis (0.153 μM **17d** in $CHCl_3$): λ_{max} (log ε) 303 (4.47), 377 (4.28), 434 (4.28), 543 (4.28), 578 (4.21), 779 (3.75). ^{1}H NMR ($CDCl_3$, 500 MHz): δ 9.76 (s, 2H, 5,20-H), 8.92 (v br, 2H, 2 × *o*-H), 8.82 (s, 2H, 12,13-H), 8.76 (d, 2H, $^3J_{HH}$ = 4.5 Hz, 7,18-H), 8.32−8.28 (m, 2H, 2^1,3^1-H), 8.25 (d, 2H, $^3J_{HH}$ = 4.5 Hz, 8,17-H), 7.57 (t, 2H, $^3J_{HH}$ = 7.4 Hz, 2 × *p*-H), 7.48−7.44 (m, 2H, 2^2,3^2-H), 7.93−7.34 (v

https://doi.org/10.1021/acs.inorgchem.1c01039
Inorg. Chem. 2021, 60, 9833−9847

br, 4H, 4 × *m*-H), 6.62 (v br, 2H, 2 × *o*-H). $\{^1H\}^{13}C$ NMR ($CDCl_3$, 125 MHz): δ 158.1, 153.0 (12,13-CH), 148.9, 144.4, 144.2, 143.4, 143.2, 143.1, 133.35 (7,18-CH), 133.31, 130.5 (8,17-CH), 128.6 (2 × *p*-CH), 128.2, 126.7 (2^2,3^2-CH), 122.1 (5,20-CH), 119.4 (2^1,3^1-CH). HR-MS (ESI) *m*/*z*: M^+ calcd for $C_{37}H_{22}N_2PdTe$, 729.9880; found, 729.9910.

Computational Studies. Calculations on structures **14a−d**, **15a−d**, **19**, **20**, **23a−d**, **24a-d**, **25**, and **26** and related protonated species were performed using Gaussian 16, Revision C.01.[33] Geometry optimization of these structures was performed with the M06-2X functional[33] by using the 6-31+G(d,p) basis set.[34] Se and Te were both modeled using the Los Alamos LANL2DZ basis.[35] Vibrational frequencies were computed to confirm the absence of imaginary frequencies to determine that the structures were minima and to derive zero-point energy and vibrational entropy corrections from unscaled frequencies. Two types of NMR calculations were performed; the GIAO method was used to obtain NICS values,[36] and CGST was used to obtain AICD plots.[27,37] NICS(0) was calculated at the mean position of all four heavy atoms in the middle of the macrocycle. NICS(a), NICS(b), NICS(c), NICS(d), and NICS(e) values were obtained by applying the same method to the mean position of the heavy atoms that comprise the individual rings of each macrocycle. In addition, $NICS(1)_{zz}$, $NICS(1a)_{zz}$, $NICS(1b)_{zz}$, $NICS(1c)_{zz}$, $NICS(1d)_{zz}$, and $NICS(1e)_{zz}$ values were obtained by applying the same method to ghost atoms placed 1 Å above each of the corresponding NICS(0) points and extracting the *zz* contribution of the magnetic tensor. The resulting Cartesian coordinates, energies, 3D geometries, and AICD plots for all the molecules can be found in the Supporting Information.

■ ASSOCIATED CONTENT

Supporting Information

The Supporting Information is available free of charge at https://pubs.acs.org/doi/10.1021/acs.inorgchem.1c01039.

Cartesian coordinates, calculated energies, selected bond lengths and AICD plots, and selected UV−vis, ^1H NMR, $^1H-^1H$ COSY, HSQC, DEPT-135, ^{13}C NMR, and mass spectra (PDF)

Accession Codes

CCDC 2051439−2051440 contain the supplementary crystallographic data for this paper. These data can be obtained free of charge via www.ccdc.cam.ac.uk/data_request/cif, or by emailing data_request@ccdc.cam.ac.uk, or by contacting The Cambridge Crystallographic Data Centre, 12 Union Road, Cambridge CB2 1EZ, UK; fax: +44 1223 336033.

■ AUTHOR INFORMATION

Corresponding Author

Timothy D. Lash − *Department of Chemistry, Illinois State University, Normal, Illinois 61790-4160, United States;* orcid.org/0000-0002-0050-0385; Email: tdlash@ilstu.edu

Authors

Deyaa I. AbuSalim − *Department of Chemistry, Illinois State University, Normal, Illinois 61790-4160, United States*

Gregory M. Ferrence − *Department of Chemistry, Illinois State University, Normal, Illinois 61790-4160, United States;* orcid.org/0000-0001-7549-3856

Complete contact information is available at: https://pubs.acs.org/10.1021/acs.inorgchem.1c01039

Notes

The authors declare no competing financial interest.

■ ACKNOWLEDGMENTS

This work was supported by the National Science Foundation under grant CHE-1855240. Further support from the National Science Foundation was obtained through the Major Research Instrumentation Program under grants CHE-1039689 (X-ray diffractometer) and CHE-0722385 (500 MHz NMR spectrometer).

■ REFERENCES

(1) Latos-Grażyński, L. Core-Modified Heteroanalogues of Porphyrins and Metalloporphyrins, in *The Porphyrin Handbook*; Kadish, K. M., Smith, K. M., Guilard, R., Eds,; Academic Press: San Diego, 2000; Vol. *2*, pp 361−416.

(2) (a) Brückner, C.; Akhigbe, J.; Samankumara, L. P. Porphyrin Analogs Containing Non-Pyrrolic Heterocycles. In *Handbook of Porphyrin Science - With Applications to Chemistry, Physics, Material Science, Engineering, Biology and Medicine*; Smith, K. M., Kadish, K. M., Guilard, R., Eds.; World Scientific: Singapore, 2014; Vol. *31*, pp 1−275. (b) Chatterjee, T.; Shetti, V. S.; Sharma, R.; Ravikanth, M. Heteroatom-Containing Porphyrin Analogues. *Chem. Rev.* **2017**, *117*, 3254−3328.

(3) Matano, Y.; Imahori, H. Phosphole-Containing Calixpyrroles, Calixphyrins, and Porphyrins: Synthesis and Coordination Chemistry. *Acc. Chem. Res.* **2009**, *42*, 1193−1204.

(4) Lash, T. D. Carbaporphyrinoid Systems. *Chem. Rev.* **2017**, *117*, 2313−2446.

(5) Ulman, A.; Manassen, J.; Frolow, F.; Rabinovich, D. Synthesis of New Tetraphenylporphyrin Molecules Containing Heteroatoms other than Nitrogen. III. Tetraphenyl-21-tellura-23-thiaporphyrin: An Internally-Bridged Porphyrin. *Tetrahedron Lett.* **1978**, *19*, 1885−1886.

(6) Latos-Grażyński, L.; Pacholska, E.; Chmielewski, P. J.; Olmstead, M. M.; Balch, A. L. Alteration of the Reactivity of a Tellurophene Within a Core-Modified Porphyrin Environment: Synthesis and Oxidation of 21-Telluraporphyrin. *Angew. Chem., Int. Ed. Engl.* **1995**, *34*, 2252−2254.

(7) (a) Abe, M.; Hilmey, D. G.; Stilts, C. E.; Sukumaran, D. K.; Detty, M. R. 21-Telluraporphyrins. 1. Impact of 21,23-Heteroatom Interactions on Electrochemical Redox Potentials, ^{125}Te NMR Spectra, and Absorption Spectra. *Organometallics* **2002**, *21*, 2986−2992. (b) Abe, M.; You, Y.; Detty, M. R. 21-Telluraporphyrins. 2. Catalysts for Bromination Reactions with Hydrogen Peroxide and Sodium Bromide. *Organometallics* **2002**, *21*, 4546−4551.

(8) Pacholska, E.; Latos-Grażyński, L. An Unorthodox Conformation of [18]porphyrin-(1.1.1.1) Heteroanalogue − 21,23-Ditelluraporphyrin with a Flipped Tellurophene Ring. *Angew. Chem., Int. Ed.* **2001**, *40*, 4466−4469.

(9) Pacholska, E.; Latos-Grażyński, L.; Ciunik, Z. A Direct Link Between Annulene and Porphyrin Chemistry − 21-Vacataporphyrin. *Chem. - Eur. J.* **2002**, *8*, 5403−5406.

(10) Pacholska-Dudziak, E.; Szterenberg, L.; Latos-Grażyński, L. A Flexible Porphyrin-Annulene Hybrid: A Nonporphyrin Conformation for meso-Tetraaryldivacataporphyrin. *Chem. - Eur. J.* **2011**, *17*, 3500−3511.

(11) Dideazaporphyrins have also been prepared by McMurry coupling of pyrrole diacrylaldehydes: (a) Lash, T. D.; Jones, S. A.; Ferrence, G. M. Synthesis and Characterization of Tetraphenyl-21.23-dideazaporphyrin: The Best Evidence Yet That Porphyrins Are the [18]Annulenes of Nature. *J. Am. Chem. Soc.* **2010**, *132*, 12786−12787. (b) Laxner, J. T.; Lash, T. D. Tetrabutyldideazaporphyrin. *Tetrahedron Lett.* **2020**, *61*, 152619.

(12) (a) Pacholska-Dudziak, E.; Szczepaniak, M.; Ksiazek, A.; Latos-Grażyński, L. *Angew. Chem., Int. Ed.* **2013**, *52*, 8898−8903. (b) Pacholska-Dudziak, E.; Vetter, G.; Góratowska, A.; Bialonska, A.; Latos-Grażyński, L. Chemistry Inside a Porphyrin Skeleton: Platinacyclopentadiene from Tellurophene. *Chem. - Eur. J.* **2020**, *26*, 16011−16018.

(13) Alka, A.; Shetti, V. S.; Ravikanth, M. Telluraporphyrinoids: An Interesting Class of Core-Modified Porphyrinoids. *Dalton Trans.* **2019**, *48*, 4444−4459.
(14) (a) Kumar, S.; Lee, W.-Z.; Ravikanth, M. Synthesis of Tellurabenziporphyrin and Its Pd(II) Complex. *Org. Lett.* **2018**, *20*, 636−639. (b) Sengupta, R.; Thorat, K. G.; Ravikanth, M. Effects if Core Modification on Electronic Properties of *para*-Benziporphyrins. *Inorg. Chem.* **2019**, *58*, 12069−12082.
(15) Ahmad, S.; Singhal, A.; Nisa, K.; Chauhan, S. M. S. Synthesis of Selenium and Tellurium Core-Modified Azuliporphyrinogens and Benziporphyrinogens and Corresponding Carbaporphyrinoids. *Inorg. Chem.* **2018**, *57*, 11333−11340.
(16) Lash, T. D. Carbaporphyrins and Related Systems. Synthesis, Characterization, Reactivity and Insights into the Nature of Porphyrinoid Aromaticity. In *Handbook of Porphyrin Science - With Applications to Chemistry, Physics, Material Science, Engineering, Biology and Medicine*; Kadish, K. M., Smith, K. M., Guilard, R., Eds.; World Scientific: Singapore, 2012; Vol. *16*, pp 1−329.
(17) Stateman, L. M.; Lash, T. D. Syntheses of Carbaporphyrinoid Systems Using a Carbatripyrrin Methodology. *Org. Lett.* **2015**, *17*, 4522−4525.
(18) Smolczyk, T. J.; Lash, T. D. Alphabet Soup Within a Porphyrinoid Cavity: Synthesis of Heterocarbaporphyrins with CNNO, CNOO, CNSO and CNSeO Cores from an Oxacarbatripyrrin. *Chem. Commun.* **2018**, *54*, 9003−9006.
(19) Lash, T. D.; Fosu, S. C.; Smolczyk, T. J.; AbuSalim, D. I. Synthesis of Expanded Porphyrinoids with Azulene and Indene Subunits and an *opp*-Dioxadicarbaporphyrin from Fulvene Carbinols and a Dioxacarbatripyrrin. *J. Org. Chem.* **2018**, *83*, 12619−12631.
(20) Lash, T. D.; Ferrence, G. M. Metalation and Selective Oxidation of Diphenyl-23-oxa-, -thia-, and Selena-21-carbaporphyrins. *Inorg. Chem.* **2017**, *56*, 11426−11434.
(21) See also: (a) Liu, D.; Lash, T. D. Synthesis, Spectroscopy and Metallation of Mixed Carbaporphyrinoid Systems. *Chem. Commun.* **2002**, *38*, 2426−2427. (b) Liu, D.; Ferrence, G. M.; Lash, T. D. Oxybenziporphyrins, Oxypyriporphyrins, Benzocarbaporphyrins, and Their 23-Oxa- and 23-Thia Analogues: Synthesis, Spectroscopic Characterization, Metalation, and Structural Characterization of a Palladium(II) Organometallic Derivative. *J. Org. Chem.* **2004**, *69*, 6079−6093.
(22) Dilute solutions of **14d** were particularly prone to air oxidation. Satisfactory spectroscopic measurements could be made so long as exposure to air was minimized. At the higher concentrations used to obtain NMR data, **14d** was reasonably stable over a period of several hours.
(23) Bruno, I. J.; Cole, J. C.; Kessler, M.; Luo, J.; Motherwell, W. D. S.; Purkis, L. H.; Smith, B. R.; Taylor, R.; Cooper, R. I.; Harris, S. E.; Orpen, A. G. Retrieval of Crystallographically-Derived Molecular Geometry Information. *J. Chem. Inf. Comput. Sci.* **2004**, *44*, 2133−2144.
(24) Lukevics, E.; Arsenyan, P.; Belyakov, S.; Pudova, O. *Chem. Heterocycl. Compd.* **2002**, *38*, 763−777.
(25) (a) Pietrasiak, E.; Togni, A. Synthesis and Characterization of Fluorinated Hypervalent Tellurium Derivatives. *Organometallics* **2017**, *36*, 3750−3757. (b) Cozzolino, A. F.; Elder, P. J. W.; Vargas-Baca, I. A Survey of Tellurium-Centered Secondary-Bonding Supramolecular Synthons. *Coord. Chem. Rev.* **2011**, *255*, 1426−1438. (c) Cozzolino, A. F.; Vargas-Baca, I.; Mansour, S.; Mahmoudkhani, A. H. The Nature of the Supramolecular Association of 1,2,5-Chalcogenadiazoles. *J. Am. Chem. Soc.* **2005**, *127*, 3184−3190.
(26) Schleyer, P. v. R.; Maerker, C.; Dransfeld, A.; Jiao, H.; van Eikema Hommes, N. J. R. Nucleus Independent Chemical Shifts: A Simple and Efficient Aromaticity Probe. *J. Am. Chem. Soc.* **1996**, *118*, 6317−6318.
(27) Geuenich, D.; Hess, K.; Kohler, F.; Herges, R. Anisotropy of the Induced Current Density (ACID), a General Method to Quantify and Visualize Electronic Delocalization. *Chem. Rev.* **2005**, *105*, 3758−3772.
(28) AbuSalim, D. I.; Lash, T. D. Relative Stability and Diatropic Character of Carbaporphyrin, Dicarbaporphyrin, Tricarbaporphyrin and Quatyrin Tautomers. *J. Org. Chem.* **2013**, *78*, 11535−11548.
(29) AbuSalim, D. I.; Lash, T. D. Aromatic Character and Relative Stability of Neo-Confused Porphyrin Tautomers and Related Compounds. *Org. Biomol. Chem.* **2013**, *11*, 8306−8323.
(30) AbuSalim, D. I.; Lash, T. D. In Pursuit of Novel Porphyrin Isomers. Aromatic Character and Relative Stability of Conjugated Tetrapyrroles with Two Neo-Confused Rings or with Mixed Neo-Confused and N-Confused Subunits. *J. Phys. Chem. A* **2015**, *119*, 11440−11453.
(31) AbuSalim, D. I.; Lash, T. D. Tropylium and Porphyrinoid Character in Carbaporphyrinoid Systems. Relative Stability and Aromatic Characteristics of Azuliporphyrin and Tropiporphyrin Tautomers, Protonated Species, and Related Species. *J. Phys. Chem. A* **2019**, *123*, 230−246.
(32) Noboa, M. A.; AbuSalim, D. I.; Lash, T. D. Azulichlorin and Benzochlorins derived Therefrom. *J. Org. Chem.* **2019**, *84*, 11649−11664.
(33) Frisch, M. J.; Trucks, G. W.; Schlegel, H. B.; Scuseria, G. E.; Robb, M. A.; Cheeseman, J. R.; Scalmani, G.; Barone, V.; Petersson, G. A.; Nakatsuji, H.; Li, X.; Caricato, M.; Marenich, A. V.; Bloino, J.; Janesko, B. G.; Gomperts, R.; Mennucci, B.; Hratchian, H. P.; Ortiz, J. V.; Izmaylov, A. F.; Sonnenberg, D. L.; Williams-Young, D.; Ding, F.; Lipparini, F.; Egidi, F.; Goings, J.; Peng, B.; Petrone, A.; Henderson, T.; Ranasinghe, D.; Zakrzewski, V. G.; Gao, J.; Rega, N.; Zheng, G.; Liang, W.; Hada, M.; Ehara, M.; Toyota, K.; Fukuda, R.; Hasegawa, J.; Ishida, M.; Nakajima, T.; Honda, Y.; Kitao, O.; Nakai, H.; Vreven, T.; Throssell, K.; Montgomery, J. A., Jr.; Peralta, J. E.; Ogliaro, F.; Bearpark, M. J.; Heyd, J. J.; Brothers, E. N.; Kudin, K. N.; Staroverov, V. N.; Keith, T. A.; Kobayashi, R.; Normand, J.; Raghavachari, K.; Rendell, A. P.; Burant, J. C.; Iyengar, S. S.; Tomasi, J.; Cossi, M.; Millam, J. M.; Klene, M.; Adamo, C.; Cammi, R.; Ochterski, J. W.; Martin, R. L.; Morokuma, K.; Farkas, O.; Foresman, J. B.; Fox, D. J. *Gaussian 16, Rev. C.01*; Gaussian, Inc.: Wallingford, CT, 2019.
(34) (a) Clark, T.; Chandrasekhar, J.; Spitznagel, G. W.; Schleyer, P. v. R. Efficient Diffuse Function−Augmented Basis Sets for Anion Calculations. III. The 3-21+G Basis Set for First−Row Elements, Li−F. *J. Comput. Chem.* **1983**, *4*, 294−301. (b) Ditchfield, R.; Hehre, W. J.; Pople, J. A. Self−Consistent Molecular−Orbital Methods. IX. An Extended Gaussian−Type Basis for Molecular−Orbital Studies of Organic Molecules. *J. Chem. Phys.* **1971**, *54*, 724−728. (c) Hariharan, P. C.; Pople, J. A. The Influence of Polarization Functions on Molecular Orbital Hydrogenation Energies. *Theor. Chim. Acta* **1973**, *28*, 213−222. (d) Hehre, W. J.; Ditchfield, R.; Pople, J. A. Self-Consistent Molecular Orbital Methods. XII. Further Extensions of Gaussian-Type Basis Sets for Use in Molecular Orbital Studies of Organic Molecules. *J. Chem. Phys.* **1972**, *56*, 2257−2261.
(35) Wadt, W. R.; Hay, P. J. *Ab initio* Effective Core Potentials for Molecular Calculations. Potentials for Main Group Elements Na to Bi. *J. Chem. Phys.* **1985**, *82*, 284−298.
(36) Chen, Z.; Wannere, C. S.; Corninboeuf, C.; Puchta, R.; Schleyer, P. v. R. Nucleus-Independent Chemical Shifts (NICS) as an Aromaticity Criterion. *Chem. Rev.* **2005**, *105* (10), 3842−3888.
(37) Herges, R.; Geuenich, D. Delocalization of Electrons in Molecules. *J. Phys. Chem. A* **2001**, *105*, 3214−3220.

https://doi.org/10.1021/acs.inorgchem.1c01039
Inorg. Chem. 2021, 60, 9833−9847